Chemical Engineering Science 131 (2015) 323–339

Contents lists available at ScienceDirect

Chemical Engineering Science

journal homepage: www.elsevier.com/locate/ces

An extended quadrature-based moment method with log-normal kernel density functions

E. Madadi-Kandjani, A. Passalacqua *

Department of Mechanical Engineering, Iowa State University, Black Engineering Building, Ames, IA 50011-2161, USA

AUTHOR-HIGHLIGHTS

- Extended quadrature-based moment method with log-normal kernel density functions.
- Solution of a population balance equation with aggregation and breakup, coalescence and breakup, condensation.
- Reconstruction of number density function.
- Study of the existence of the EQMOM solution.
- Validation against rigorous solution.

ARTICLE INFO

Article history:
Received 25 December 2014
Received in revised form
23 March 2015
Accepted 6 April 2015
Available online 14 April 2015

Keywords:
Extended quadrature method of moments
Log-normal kernel density function
Population balance equation
Aggregation and breakup
Coalescence
Condensation

ABSTRACT

An extended quadrature method of moments (EQMOM) with log-normal kernel density functions is developed in this work, and applied to the solution of a population balance equation (PBE) for aggregation and breakup, coalescence, and condensation problems. The cases with one and two kernel density functions are studied analytically, and the existence of an analytical solution is shown. A numerical procedure based on the work of Yuan et al. (2012) is adopted to address cases with a larger number of kernel density functions. Results for the reconstructed number density function (NDF), the time evolution of the zero-order moment and of the mean particle size are compared with those obtained from the rigorous solution of the PBE reported by Vanni (2000) for the cases of aggregation and breakup. A problem concerning coalescence and one regarding condensation, both with analytical solution, are also examined. The results obtained with the proposed approach are compared to those provided by EQMOM with gamma kernel densities. Satisfactory results were obtained for the reconstructed distribution. Excellent agreement was observed between the rigorous solution and the approximated one for the time evolution of the total number density and the mean particle size.

1. Introduction

Numerous environmental, biological, medical, and technological systems involve discrete populations of particles, whose properties evolve in space and time due to continuous phenomena, such as convection and diffusion, and discontinuous phenomena, such as aggregation, breakup, nucleation, evaporation, coalescence. Notable examples are polymerization processes, dispersion of aerosols in the atmosphere, chemical reactions involving precipitation of particles, bubble column reactors, processes for the production of pharmaceuticals. The evolution of the particle population in these systems is modeled by means of a population balance equation (PBE) (Ramkrishna, 2000), which is an integro-differential equation, whose unknown is the number density function (NDF) associated to the particle population. This NDF depends, in general, on time, on a set of external coordinates, representing the spatial location, and on a set of internal coordinates, which characterize the particle properties.

In this work we concentrate on the case of a NDF with only one internal coordinate, representing the particle size. Numerous methods were developed to solve this type of equation. Balakin et al. (2014), Bannari et al. (2008), Becker et al. (2011), Hounslow et al. (1988), Hounslow (1990), Kumar and Ramkrishna (1996a,b), and Puel et al. (2003) used the method of classes, which consists in discretizing the NDF with respect to the internal coordinate using a discrete number of bins (classes). Zero-order class methods assume a uniform distribution for each bin (Vanni, 2000), while high-order class methods adopt a pre-defined functional form of the distribution for each class (Muhr et al., 1996). Bove et al. (2005) developed the parallel parent and daughter class (PPDC) approach

* Corresponding author.
E-mail address: albertop@iastate.edu (A. Passalacqua).

http://dx.doi.org/10.1016/j.ces.2015.04.005
0009-2509/

for aggregation and breakup problems. Alopaeus et al. (2006) developed a high-order moment-conserving class method to overcome the limitations of traditional class methods (Hounslow et al., 1988; Hounslow, 1990; Kumar and Ramkrishna, 1996a,b), which conserve only two moments in the discrete solution for the PBE for agglomeration and breakup. This approach was combined with a reconstruction procedure of the NDF by Alopaeus et al. (2008).

The method of classes, while intuitive and accurate, is computationally intensive due to the large number of classes required to properly discretize the NDF (Marchisio et al., 2003). Lin et al. (2002), Meimaroglou and Kiparissides (2007), Rosner and Yu (2001), Smith and Matsoukas (1998), Zhao et al. (2007), and Zhao and Zheng (2013) used Monte Carlo methods to tackle the PBE. Hulburt and Katz (1964) solved the PBE with the standard method of moments (SMM), accurately predicting the evolution of the NDF with size-independent growth rate, aggregation and breakup terms.

A successful approach to find an approximate solution to population balance equations is the quadrature method of moments (QMOM) proposed by McGraw (1997) for aerosol applications, and extensively used in typical applications of chemical engineering (Marchisio and Fox, 2013). In this approach the NDF is represented by a weighted summation of Dirac delta functions, which is uniquely defined by the set of moments (Gordon, 1968; Wheeler, 1974).

The discrete representation of the NDF was used in the direct quadrature method of moments (DQMOM) (Marchisio and Fox, 2005) to derive transport equations for the quadrature weights and abscissae. However, shortcomings related to the conservation of moments affect the DQMOM approach, due to the fact that weights and abscissae are not conserved quantities, as mentioned in Yuan et al. (2012).

The accuracy of QMOM, DQMOM and PPDC were compared by Silva et al. (2010), who concluded that QMOM and DQMOM show similar accuracy in the aggregation and breakup problems considered in their work, while the PPDC approach showed convergence difficulties and its accuracy was not adequate.

In general, a method relying on a discrete representation of the NDF is also affected by limitations that become particularly relevant in some classes of problems. For example, some evaporation problems (Fox et al., 2008; Yuan et al., 2012) require the value of the NDF for null internal coordinate to be known, which is not the case if the QMOM discretization of the NDF is used. This challenge can only be effectively overcome with methods that rely on a continuous representation of the distribution function. One of these methods is the entropy maximization approach (Mead and Papanicolaou, 1984; Tagliani, 1999), which is ill-posed when the moment set is too large, or it is near the boundary of the moment space. The first problem was successfully addressed in Vie et al. (2013), while the second one is typical of moment methods. The entropy maximization method can also be extended to multivariate problems, if a sufficient number of moments of the NDF are considered (Massot et al., 2010). However, in practical applications, the computational cost of entropy-maximization methods can be higher than the one of quadrature-based moment methods (Kah et al., 2012).

Strumendo and Arastoopour (2008) proposed to use the finite-size domain complete set of trial functions method of moments (FCMOM) to approximate the solution of the PBE. In this approach, Legendre polynomials are used to obtain a continuous reconstruction of the NDF. However, as explained in Yuan et al. (2012), this approach cannot guarantee the positivity of the reconstructed NDF due to the finite number of polynomials that can be determined from the finite set of transported moments. This limitation may likely lead to non-realizable moment sets, in particular when solving inhomogeneous problems (Wright, 2007; Yuan et al., 2012). An alternative method was proposed by Athanassoulis and Gavriliadis (2002), who introduced the idea of reconstructing the NDF as a finite superposition of kernel density functions. Important advantages of this approach are that it ensures positivity of the reconstructed NDF, and it converges to the exact NDF when the number of kernel density functions used in the reconstruction is increased (Athanassoulis and Gavriliadis, 2002). The approach of Athanassoulis and Gavriliadis (2002), however, relies on the solution of a minimization problem, which only guarantees that some of the low-order moments are exactly preserved (Yuan et al., 2012).

In order to overcome this limitation, Chalons et al. (2010) and Yuan et al. (2012) introduced an extended quadrature method of moments (EQMOM), where continuous non-negative kernel density functions are used in place of Dirac delta functions, when approximating the NDF. This allows an approximate continuous distribution function to be determined from the transported moments. Additionally, the EQMOM procedure ensures that the reconstructed NDF preserves all the moments used for its reconstruction. The approximated NDF obtained with EQMOM can then be used to integrate the source terms in the population balance equation in a more accurate manner (Marchisio and Fox, 2013). Chalons et al. (2010) formulated the method using Gaussian kernel density functions, while Yuan et al. (2012) used beta and gamma density functions.

The present work proposes an extended quadrature method of moments using log-normal kernel density functions. Log-normal distribution functions are frequently encountered in many geological, medical, environmental (Limpert et al., 2001) and industrial (Randolph and Larson, 1988; Petitti et al., 2010; Capecelatro et al., 2014) applications involving particles, bubbles and droplets. As a consequence, being able to use log-normal kernel density functions may improve the efficiency of the EQMOM procedure in cases where distributions are nearly log-normal, reducing the number of kernel density functions required to achieve a satisfactory reconstruction. Additionally, it will be illustrated that the structure of the system of equations to be solved in the EQMOM procedure is particularly simple when log-normal kernel density functions are chosen. The cases with one and two kernel density functions are studied analytically. The existence of a solution to the moment inversion and reconstruction problem is shown for these cases. The problem of moment realizability is studied for the case with two kernel density functions. The proposed procedure is then tested considering cases involving aggregation and breakup (Vanni, 2000), coalescence and breakup, and condensation (Lage, 2011; Yuan et al., 2012). The effect of time integration on the accuracy of the steady-state reconstructed distribution was investigated for the cases where the rigorous solution of the PBE was available in the literature (Vanni, 2000). This was achieved by numerically integrating the NDF obtained from the rigorous solution of the PBE to compute its moments, and using these moments to perform the EQMOM reconstruction.

The remainder of the paper is structured as follows: Section 2 briefly summarizes the theory of population balance equations, while Section 3 introduces the details of EQMOM and focuses on formulating the extended quadrature method of moments with log-normal kernel density functions (LnEQMOM). In particular, analytical solutions for the case with one and two quadrature nodes are discussed, and a numerical solution procedure (Yuan et al., 2012) is illustrated for the general case with N kernel density functions. Section 4 illustrates a verification study performed on the proposed procedure (Section 4.1), presents the results concerning the solution of the PBE for aggregation and breakup problems (Section 4.2), coalescence (Section 4.3) and condensation (Section 4.4) and discusses the problem of moment realizability

for the EQMOM procedure with two log-normal kernel density functions (Section 4.5). Finally, Section 5 analyses the computational cost of the EQMOM procedure in comparison to QMOM.

2. PBE for aggregation and breakup problem

The population balance equation (Ramkrishna, 2000; Vanni, 2000) accounting for the evolution of the number density function only due to birth and death of particles can be written as

$$\frac{\partial n(\xi,t)}{\partial t}=\overline{B}(\xi,t)-\overline{D}(\xi,t), \tag{1}$$

where $n(\xi,t)$ is the number density function, depending on the single internal coordinate ξ, while $\overline{B}(\xi,t)$ and $\overline{D}(\xi,t)$ are, respectively, the rate of change of n due to birth and death. The internal coordinate ξ represents a characteristic dimension of the particle (diameter, volume, etc.). The specific meaning will be clarified for each case. Both these terms are usually decomposed in the algebraic sum of the contributions due to aggregation and breakup to birth and death of particles of a given size, leading to

$$\frac{\partial n(\xi,t)}{\partial t}=\overline{B}^{a}(\xi,t)-\overline{D}^{a}(\xi,t)+\overline{B}^{b}(\xi,t)-\overline{D}^{b}(\xi,t). \tag{2}$$

It is worth noting that the internal coordinate ξ represents a characteristic property of the particle related to its size, such as the particle diameter or its mass. We will consider ξ as the particle size in the aggregation and breakup problems, while ξ will represent the particle mass in the two problems concerning coalescence and condensation considered in this work. According to previous studies (Marchisio and Fox, 2013; Marchisio et al., 2003; Randolph and Larson, 1988), these terms can be written in a continuous form for a homogeneous system as

$$\overline{B}^{a}(\xi,t)=\frac{\xi^2}{2}\int_0^{\xi}\frac{\beta\left(\left(\xi^3-\xi'^3\right)^{1/3},\xi'\right)}{\left(\xi^3-\xi'^3\right)^{2/3}}n\left(\left(\xi^3-\xi'^3\right)^{1/3},t\right)n(\xi',t)\,\mathrm{d}\xi', \tag{3}$$

$$\overline{D}^{a}(\xi,t)=n(\xi,t)\int_0^{\infty}\beta(\xi,\xi')n(\xi',t)\,\mathrm{d}\xi', \tag{4}$$

$$\overline{B}^{b}(\xi,t)=\int_{\xi}^{\infty}a(\xi')b(\xi|\xi')n(\xi',t)\,\mathrm{d}\xi', \tag{5}$$

$$\overline{D}^{b}(\xi,t)=a(\xi)n(\xi,t). \tag{6}$$

The aggregation kernel β describes the probability of particles to aggregate, and can be expressed as a product of the collision frequency and the aggregation efficiency, $a(\xi)$ is the breakup kernel and $b(\xi|\xi')$ is the fragmentation distribution function that contains information on the fragments produced by a breakup event (Marchisio et al., 2003). The reader interested in how to derive Eqs. (3)–(6) can refer to Marchisio et al. (2003) for further details.

3. The extended quadrature method of moments

The solution of the PBE with the extended quadrature method of moments requires moment transport equations to be obtained from Eq. (2). This is achieved by applying the definition of the moment of order k of the NDF

$$M_k(t)=\int_0^{\infty}n(\xi,t)\xi^k\,\mathrm{d}\xi \tag{7}$$

to each side of the PBE (Eq. (2)), leading to

$$\frac{\partial M_k(t)}{\partial t}=\overline{B}_k^{a}(t)-\overline{D}_k^{a}(t)+\overline{B}_k^{b}(t)-\overline{D}_k^{b}(t). \tag{8}$$

The source terms due to birth and death as a consequence of aggregation and breakup phenomena are defined as the moments of the source terms in the original PBE, as follows:

$$\begin{aligned}
\overline{B}_k^{a}(t)&=\frac{1}{2}\int_0^{\infty}n(\xi',t)\int_0^{\infty}\beta(\xi,\xi')\left(\xi^3+\xi'^3\right)^{k/3}n(\xi,t)\,\mathrm{d}\xi\,\mathrm{d}\xi',\\
\overline{D}_k^{a}(t)&=\int_0^{\infty}\xi^k n(\xi,t)\int_0^{\infty}\beta(\xi,\xi')n(\xi',t)\,\mathrm{d}\xi'\,\mathrm{d}\xi,\\
\overline{B}_k^{b}(t)&=\int_0^{\infty}\xi^k\int_0^{\infty}a(\xi')b(\xi|\xi')n(\xi',t)\,\mathrm{d}\xi'\,\mathrm{d}\xi,\\
\overline{D}_k^{b}(t)&=\int_0^{\infty}\xi^k a(\xi)n(\xi,t)\,\mathrm{d}\xi.
\end{aligned} \tag{9}$$

The evaluation of the integrals in Eq. (9) requires the knowledge of the NDF, in addition to the kernel functions a and β. However, the NDF is not known a priori, and has to be approximated from the transported moments.

Following the procedure described in Yuan et al. (2012), we choose to approximate the NDF with a weighted sum of non-negative kernel density functions $\delta_\sigma(\xi,\xi_\alpha)$:

$$n(\xi)\approx p_N(\xi)=\sum_{\alpha=1}^{N}w_\alpha\delta_\sigma(\xi,\xi_\alpha), \tag{10}$$

where w_α are the non-negative weights of each kernel density function, ξ_α are the corresponding quadrature abscissae, and N is the number of kernel density functions used to approximate the NDF. Since the particle size is a positive, real number, the support of the kernel density function δ_σ is chosen to be the whole real positive axis $\mathbb{R}^+$.

The approximation introduced with Eq. (10) allows the calculation of the integrals that appear in the source terms of Eq. (9) to be carried out. After substituting the equation for $p_N(\xi)$, and approximating the integrals with quadrature formulae, the following expression is obtained (Yuan et al., 2012):

$$\begin{aligned}
\int_0^{\infty}g(\xi)p_N(\xi)\,\mathrm{d}\xi&=\int_0^{\infty}g(\xi)\sum_{\alpha=1}^{N}w_\alpha\delta_\sigma(\xi,\xi_\alpha)\,\mathrm{d}\xi\\
&=\sum_{\alpha=1}^{N}\sum_{\beta=1}^{N_\alpha}w_\alpha w_{\alpha\beta}g\left(\xi_{\alpha\beta}\right).
\end{aligned} \tag{11}$$

The N *primary* weights w_α, the corresponding primary abscissae ξ_α, together with the parameter σ are determined from the first $2N+1$ integer moments of the NDF, as illustrated in Section 3.1. The $2N_\alpha$ quantities $w_{\alpha\beta}$ and $\xi_{\alpha\beta}$, called *secondary* weights and abscissae, respectively, are computed using the standard Gaussian quadrature formulae for known orthogonal polynomials to the kernel NDF. This allows each kernel density function to be evaluated at an arbitrary number of points, depending on the desired level of accuracy.

Introducing the approximated integrals of the source terms into Eq. (9) leads to the following semi-discrete form of the moment transport equations, where $\beta_{\alpha_1\beta_1\alpha_2\beta_2}$ is the aggregation kernel for the particles of size $\xi_{\alpha_1\beta_1}$ and $\xi_{\alpha_2\beta_2}$, $a_{\alpha\beta}$ is the breakage kernel for the particle size of $\xi_{\alpha\beta}$, and $b_{\alpha\beta}$ represents the fragmentation distribution function:

$$\begin{aligned}
\frac{\partial M_k}{\partial t}=&\frac{1}{2}\sum_{\alpha_1=1}^{N}\sum_{\beta_1=1}^{N_\alpha}w_{\alpha_1}w_{\alpha_1\beta_1}\sum_{\alpha_2=1}^{N}\sum_{\beta_2=1}^{N_\alpha}w_{\alpha_2}w_{\alpha_2\beta_2}\left(\xi_{\alpha_1\beta_1}^3+\xi_{\alpha_2\beta_2}^3\right)^{k/3}\\
&\times\beta_{\alpha_1\beta_1\alpha_2\beta_2}-\sum_{\alpha_1=1}^{N}\sum_{\beta_1=1}^{N_\alpha}\xi_{\alpha_1\beta_1}^k w_{\alpha_1}w_{\alpha_1\beta_1}\sum_{\alpha_2=1}^{N}\sum_{\beta_2=1}^{N_\alpha}w_{\alpha_2}w_{\alpha_2\beta_2}\\
&\times\beta_{\alpha_1\beta_1\alpha_2\beta_2}
\end{aligned}$$

$$+\sum_{\alpha=1}^{N}\sum_{\beta=1}^{N_\alpha} w_\alpha a_{\alpha\beta}\overline{b}^{k}_{\alpha\beta} w_{\alpha\beta} - \sum_{\alpha=1}^{N}\sum_{\beta=1}^{N_\alpha} w_\alpha \xi^{k}_{\alpha\beta} a_{\alpha\beta} w_{\alpha\beta}. \tag{12}$$

3.1. The EQMOM numerical procedure

The numerical procedure to solve Eq. (12) is illustrated in this section. The starting point to define the EQMOM numerical solution procedure is to choose the functional form of the kernel density function. The choice is made based on the support of the NDF that has to be reconstructed. In other words, if the reconstructed NDF has support $\mathbb{R}$, Gaussian kernel functions may be used, while if the support is $\mathbb{R}_0^+$, gamma or log-normal kernel functions can be chosen. Beta kernel functions are suitable to reconstruct an NDF with bounded support (Yuan et al., 2012). As we mentioned in the introduction, we deal with the log-normal kernel density function in this work, which we write as:

$$\delta_\sigma(\xi,\mu) = \frac{1}{\xi\sigma\sqrt{2\pi}}\, e^{-(\ln\xi-\mu)^2/2\sigma^2}, \quad \xi,\sigma\in\mathbb{R}^+,\ \mu\in\mathbb{R}. \tag{13}$$

The integer moment of order k of the log-normal distribution can be found analytically using the Mellin transform, leading to (Magnus et al., 1966):

$$M_k(\mu,\sigma) = e^{k\mu+k^2\sigma^2/2}. \tag{14}$$

3.2. The one-node case

The case when only one kernel density function is used is trivial, and an analytical solution can be found for σ. To this purpose, it suffices to consider the first three moments of the NDF $\{M_0, M_1, M_2\}$, and impose that the moments of the approximated NDF:

$$p_1(\xi) = w_1\delta_\sigma(\xi,\xi_1) = \frac{w_1}{\xi\sigma\sqrt{2\pi}}\, e^{-(\ln\xi-\xi_1)^2/2\sigma^2} \tag{15}$$

are equal. This leads to the following non-linear system of equations:

$$\begin{cases} M_0 = w_1 \\ M_1 = w_1 e^{\xi_1+\sigma^2/2} \\ M_2 = w_1 e^{2\xi_1+2\sigma^2} \end{cases}, \tag{16}$$

which can be solved analytically by setting $z = e^{\sigma^2/2}$, and $\chi_1 = e^{\xi_1}$. Eliminating w_1 and ξ_1, and taking the only positive z root leads to:

$$z = \frac{1}{M_1}\sqrt{M_0M_2} \Rightarrow \sigma^2 = 2\ln\left(\frac{1}{M_1}\sqrt{M_0M_2}\right), \tag{17}$$

which is always defined because the moments of the NDF are strictly positive, and $M_0M_2 > M_1^2$ to ensure $\sigma^2 > 0$. The complete solution for the one-node case is then:

$$\begin{cases} w_1 = M_0 \\ \xi_1 = \ln\dfrac{M_1^2}{M_0\sqrt{M_0M_1}} \\ \sigma = \sqrt{2\ln\left(\dfrac{1}{M_1}\sqrt{M_0M_2}\right)}. \end{cases} \tag{18}$$

3.3. The two-node case

The two-node case is obtained when two kernel density functions are used to approximate the NDF. Following Chalons et al. (2010), the approximated NDF is written as

$$p_2(\xi) = w_1\delta_\sigma(\xi,\xi_1) + w_2\delta_\sigma(\xi,\xi_2)$$

$$= \frac{w_1}{\xi\sigma\sqrt{2\pi}}\, e^{-(\ln\xi-\xi_1)^2/2\sigma^2} + \frac{w_2}{\xi\sigma\sqrt{2\pi}}\, e^{-(\ln\xi-\xi_2)^2/2\sigma^2}. \tag{19}$$

It is worth reminding at this time that the parameter σ is assumed to be the same for both the kernel density functions, in order to obtain a single non-linear equation for σ, rather than a system of non-linear equations, which would significantly increase the complexity of the problem (Chalons et al., 2010; Yuan et al., 2012). The effect of this assumption on the accuracy of the reconstructed NDF is shown in Section 4.1.

The following non-linear system of equations is found imposing that the first five transported moments are exactly represented by the approximated NDF (Chalons et al., 2010):

$$\begin{cases} M_0 = w_1 + w_2 \\ M_1 = w_1 e^{\xi_1+\sigma^2/2} + w_2 e^{\xi_2+\sigma^2/2} \\ M_2 = w_1 e^{2(\xi_1+\sigma^2)} + w_2 e^{2(\xi_2+\sigma^2)} \\ M_3 = w_1 e^{3\xi_1+9/2\sigma^2} + w_2 e^{3\xi_2+9/2\sigma^2} \\ M_4 = w_1 e^{4\xi_1+8\sigma^2} + w_2 e^{4\xi_2+8\sigma^2}. \end{cases} \tag{20}$$

Setting

$$z = e^{\sigma^2/2}, \quad \chi_1 = e^{\xi_1}, \quad \chi_2 = e^{\xi_2} \tag{21}$$

leads to

$$\begin{cases} M_0 = w_1 + w_2 = M_0^* \\ M_1 = z(w_1\chi_1 + w_2\chi_2) = zM_1^* \\ M_2 = z^4(w_1\chi_1^2 + w_2\chi_2^2) = z^4M_2^* \\ M_3 = z^9(w_1\chi_1^3 + w_2\chi_2^3) = z^9M_3^* \\ M_4 = z^{16}(w_1\chi_1^4 + w_2\chi_2^4) = z^{16}M_4^*. \end{cases} \tag{22}$$

It is immediately apparent that Eq. (22), which relates the transported moments M_k to the moments of the approximated NDF M_k^*, shows a simpler structure than the corresponding system for EQMOM based on gamma kernel densities (Yuan et al., 2012). In particular, the system of equations in Eq. (22) is diagonal, while the one for gamma EQMOM is lower-triangular, as described in Yuan et al. (2012). This property is also maintained for the cases with $N > 2$.

Eliminating w_1, ξ_1, w_2, ξ_2 from Eq. (22), the following polynomial equation is found:

$$f(z) = M_2^3z^8 - 2M_1M_2M_3z^6 + \left(M_0M_3^2 + M_1^2M_4\right)z^2 - M_0M_2M_4 = 0. \tag{23}$$

Recalling that all the moments of our NDF are positive quantities, the application of Descartes rule of signs shows that this polynomial equation has a maximum of three positive real roots and of three negative roots.

We now show that at least a positive real root σ exists for Eq. (23), if the moments are positive. To this purpose, we observe that the coefficient of the leading power of the polynomial in Eq. (23) is positive because $M_2 > 0$. This implies that $\lim_{z\to+\infty} f(z) = +\infty$. We also note that $f(z=0) = -M_0M_2M_4 < 0$. As a consequence, because $f \in C^0(\mathbb{R})$, we conclude that at least one value of $z \in \mathbb{R}^+$ so that $f(z) = 0$.

We also observe that, in general, it is not possible to show that such a root is unique, as discussed before. Only additional constraints on the moment realizability may further limit the number of real roots. Analytical expressions for the real roots of Eq. (23) can be found by solving Eq. (23), and obtaining the corresponding square roots of the result. However, the complexity of the expressions obtained with this procedure makes them unpractical, and a numerical solution is favored in this work, as illustrated for the general case in Section 3.4.

3.4. The general case

The general case with N kernel density functions is treated in the same way illustrated for the two-node case. An equation for z is found imposing that the first $2N+1$ moments are exactly represented by the approximated NDF, leading to the polynomial expression

$$J_{2N}(z) = M_{2N} - z^{(2N)^2} M^*_{2N}, \tag{24}$$

where

$$M^*_{2N} = \sum_{\alpha=1}^{N} w_\alpha \chi_\alpha^{2N}. \tag{25}$$

It is worth noting that the $2N+1$ equations are coupled, since the values of both w_α and χ_α depend on z. Such a system can be solved iteratively as illustrated in Yuan et al. (2012), and briefly summarized below:

1. Guess σ, and compute the corresponding value of $z = e^{\sigma^2/2}$.
2. Compute $M^*_k = M_k z^{-(2k)^2}, k = 0, \ldots, 2N-1$ moments, using the guessed value for z.
3. Apply the Wheeler (1974) algorithm to the first $2N$ M^* moments to obtain the weights w_α and the abscissae χ_α.
4. Compute M^*_{2N} with the new values of weights and abscissae.
5. Construct the $J(z)$ function, and determine z with a bounded numerical root finding procedure.
6. Repeat from 2 until $|J(z)| < \varepsilon$, with ε being a small value close to machine precision.

Table 1
Parameters used in the cases concerning the linear combination of two log-normal distributions.

Case	μ_1	σ_1	μ_2	σ_2
1	3	0.6	3	0.6
2	1.2	0.6	3	0.6
3	3	0.6	5	0.5
4	3	0.6	1	0.8

Gaussian quadrature formulae with log-normal weight function can be computed with two approaches, which we briefly summarize in Appendix A, referring the interested reader to Gautschi (2004), Wilck (2001), and Weisstein (1998) for further details. We compared the numerical results obtained with both Hermite and Stieltjes–Wigert quadrature formulae (comparison not reported here), and we did not find significant differences for the cases discussed in this work. As a consequence, we used Hermite quadrature to approximate the integrals in the source terms of the PBE. This choice also makes the numerical procedure more efficient, because the algorithm to compute Hermite quadrature weights and nodes does not involve the parameter σ, as opposed to the one for the Stieltjes–Wigert quadrature.

4. Results and discussion

4.1. Verification of the Ln-EQMOM implementation

We verify the numerical procedure to reconstruct the NDF with LnEQMOM by considering a distribution obtained as a linear combination of two log-normal distributions with different parameters μ and σ. The functional form of this distribution is shown as

$$f(x) = \frac{1}{2}\left[\frac{1}{x\sigma_1\sqrt{2\pi}} e^{-(\ln x-\mu_1)^2/2\sigma_1^2} + \frac{1}{x\sigma_2\sqrt{2\pi}} e^{-(\ln x-\mu_2)^2/2\sigma_2^2}\right], \tag{26}$$

while the values of the parameters used in each case are summarized in Table 1. The reconstructed distributions obtained with four-node LnEQMOM are reported in Fig. 1. As expected, the reconstruction obtained in case 1 exactly matches the analytical solution, because the exact distribution is log-normal. We observe that, in general, the reconstructed distribution agrees well with the analytical function. However, as it is clear from Fig. 1(d), the agreement deteriorates for increasingly different values of the parameter σ. This is a consequence of the assumption that the kernel density functions used to define the approximated distribution (Eq. (10)) share the same value of σ.

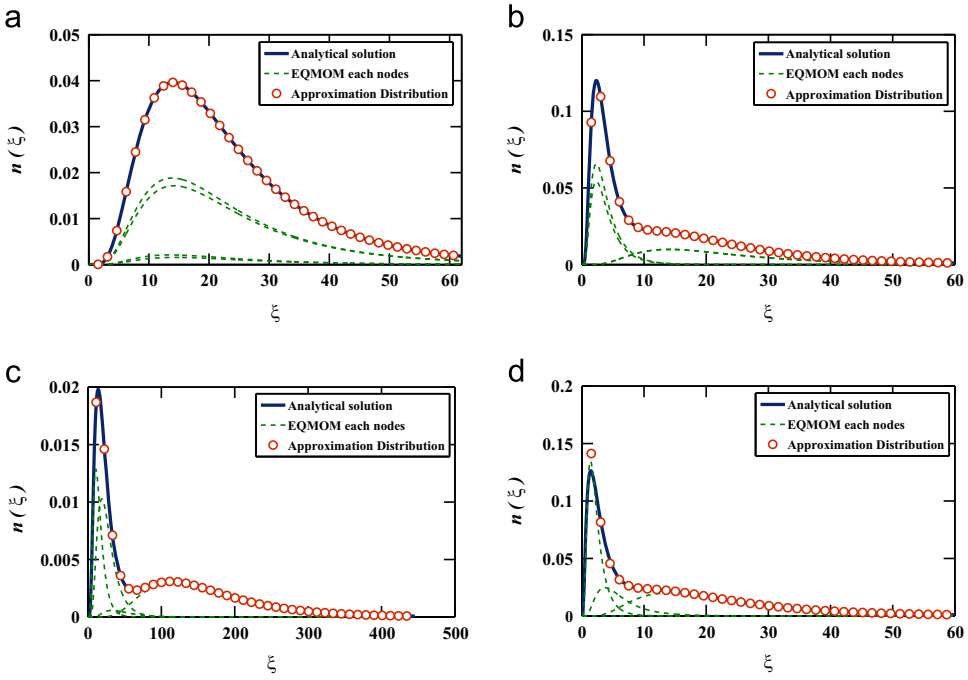

Fig. 1. Comparison between the analytical and the approximated distribution obtained with LnEQMOM using four primary quadrature nodes ($N=4$) for cases 1–4.

We first verify that the moments of the reconstructed distributions match the moments of the analytical one. To this purpose, we consider the relative error affecting the moments, defined as

$$E_i = \left| \frac{M_{i,\text{analytical}} - M_{i,\text{reconstruction}}}{M_{i,\text{analytical}}} \right|. \quad (27)$$

As shown in Table 2, the first $2N+1$ moments are preserved by EQMOM with errors of the order of $1.0 \cdot 10^{-16}$ for cases 1–3, and with errors of the order of $1.0 \cdot 10^{-12}$ for case 4. It is worth noticing that the EQMOM procedure can preserve $2N+1$ moments only when a value of the parameter σ can be found. In other words, it is possible that the equation $J_{2N}(z)=0$ does not have a root. In such cases, the EQMOM procedure will only preserve $2N$ moments, exactly as the standard QMOM approach.

We then consider the L^2 norm of the difference between the analytical distribution function and the approximated one, normalized with respect to M_0:

$$d = \frac{\| f(\xi) - p(\xi) \|_2}{M_0}. \quad (28)$$

As shown in Table 3, d is between $6.04 \cdot 10^{-16}$ ($N=4$) and $1.90 \cdot 10^{-13}$ ($N=2$) for case 1, when the analytical distribution is itself log-normal. The error is between $3.90 \cdot 10^{-14}$ ($N=4$) and $2.88 \cdot 10^{-12}$ ($N=2$) in case 2, when $\sigma_1 = \sigma_2$, with different values of μ_1 and μ_2. However, a significantly larger error (order between 10^{-3} and 10^{-1}) is observed when different values of σ_1 and σ_2 are chosen. We can also observe that the error increases when the difference between σ_1 and σ_2 increases, as expected as a consequence of the assumption that kernel densities share the same value of σ. Finally, we notice that increasing the number of primary quadrature nodes from two to four reduces the relative error of one order of magnitude in cases 1–3, but only marginally affects the error in case 4.

Table 2
Relative error affecting the moments of the reconstructed distribution as a function of the number of primary nodes N.

Case	$N=2$		$N=3$		$N=4$	
1	E_0	1.34×10^{-16}	E_0	1.41×10^{-16}	E_0	4.36×10^{-16}
	E_1	1.48×10^{-16}	E_1	1.48×10^{-16}	E_1	1.47×10^{-16}
	E_2	2.74×10^{-16}	E_2	2.74×10^{-16}	E_2	2.74×10^{-16}
	E_3	8.88×10^{-16}	E_3	8.88×10^{-16}	E_3	8.88×10^{-16}
	E_4	9.64×10^{-16}	E_4	9.64×10^{-16}	E_4	9.64×10^{-16}
			E_5	2.03×10^{-16}	E_5	2.03×10^{-16}
			E_6	3.56×10^{-16}	E_6	3.56×10^{-16}
					E_7	2.18×10^{-16}
					E_8	4.12×10^{-16}
2	E_0	1.35×10^{-16}	E_0	1.37×10^{-16}	E_0	4.35×10^{-16}
	E_1	1.27×10^{-16}	E_1	1.27×10^{-16}	E_1	1.27×10^{-16}
	E_2	2.67×10^{-16}	E_2	2.67×10^{-16}	E_2	2.67×10^{-16}
	E_3	8.84×10^{-16}	E_3	8.84×10^{-16}	E_3	8.84×10^{-16}
	E_4	9.63×10^{-16}	E_4	9.63×10^{-16}	E_4	9.63×10^{-16}
			E_5	2.03×10^{-16}	E_5	2.03×10^{-16}
			E_6	1.78×10^{-16}	E_6	1.78×10^{-16}
					E_7	2.19×10^{-16}
					E_8	4.12×10^{-15}
3	E_0	1.48×10^{-16}	E_0	1.97×10^{-16}	E_0	2.71×10^{-16}
	E_1	1.47×10^{-16}	E_1	1.48×10^{-16}	E_1	1.48×10^{-16}
	E_2	2.22×10^{-16}	E_2	2.22×10^{-16}	E_2	2.22×10^{-16}
	E_3	4.36×10^{-16}	E_3	4.36×10^{-16}	E_3	4.36×10^{-16}
	E_4	6.08×10^{-16}	E_4	6.08×10^{-16}	E_4	6.08×10^{-16}
			E_5	7.81×10^{-16}	E_5	7.81×10^{-16}
			E_6	8.21×10^{-16}	E_6	8.21×10^{-16}
					E_7	1.30×10^{-16}
					E_8	1.87×10^{-16}
4	E_0	1.34×10^{-15}	E_0	1.40×10^{-15}	E_0	4.36×10^{-15}
	E_1	1.28×10^{-14}	E_1	1.28×10^{-14}	E_1	1.27×10^{-12}
	E_2	2.66×10^{-14}	E_2	2.66×10^{-14}	E_2	2.66×10^{-12}
	E_3	8.81×10^{-14}	E_3	8.81×10^{-14}	E_3	8.81×10^{-12}
	E_4	9.61×10^{-14}	E_4	9.61×10^{-14}	E_4	9.61×10^{-12}
			E_5	2.02×10^{-14}	E_5	2.02×10^{-12}
			E_6	3.56×10^{-14}	E_6	3.56×10^{-12}
					E_7	2.19×10^{-12}
					E_8	4.12×10^{-12}

4.2. PBE for aggregation and breakup problems

We discuss in this section the solution of the PBE for aggregation and breakup problems. We refer to the work of Vanni (2000), who reported the rigorous solution for the aggregation and breakup problems considered here. In particular, we study the five cases summarized in Table 4, where the kernels for aggregation and breakup reported in Tables 5 and 6 were used, together with the daughter distribution functions listed in Table 7.

Table 3
Normalized L^2 norm of the difference d between the analytical and the approximated distribution.

Case	$N=2$	$N=3$	$N=4$
1	1.90×10^{-13}	2.21×10^{-14}	6.04×10^{-16}
2	2.88×10^{-12}	3.93×10^{-14}	3.90×10^{-14}
3	2.68×10^{-2}	6.68×10^{-3}	2.04×10^{-3}
4	2.76×10^{-1}	1.10×10^{-1}	1.07×10^{-1}

Table 4
Cases examined for the aggregation and breakup process.

Case	$\beta(\xi,\xi')$	$a(\xi)$	$b(\xi\|\xi')$	$M_k(t=0)$
5	1	$\begin{cases} 0 & \xi=1 \\ 0.02 & \xi>1 \end{cases}$	1, Table 7	$M_k=1, k=0,\ldots,6$
6	$\xi^3+\xi'^3$	$\begin{cases} 0 & \xi=1 \\ 0.02\xi^3 & \xi>1 \end{cases}$	1, Table 7	$M_k=1, k=0,\ldots,6$
7	$(\xi+\xi')^3$	$\begin{cases} 0 & \xi=1 \\ 0.1e^{0.01\xi^3} & \xi>1 \end{cases}$	1, Table 7	$M_k=1, k=0,\ldots,6$
8	$(\xi+\xi')^2\lvert\xi^2-\xi'^2\rvert$	$\begin{cases} 0 & \xi=1 \\ 0.01\xi^6 & \xi>1 \end{cases}$	2, Table 7	$\begin{cases} M_0=1 \\ M_1=1.13 \\ M_2=1.294 \\ M_3=1.5 \\ M_4=1.760 \\ M_5=2.087 \\ M_6=2.087 \end{cases}$
9	$(\xi+\xi')^3$	$\begin{cases} 0 & \xi<\sqrt[3]{5} \\ 0.1e^{0.01\xi^3} & \xi\geq\sqrt[3]{5} \end{cases}$	3, Table 7	$M_k=1, k=0,\ldots,6$

Table 5
Aggregation kernels.

Kernel	$\beta(\xi,\xi')$
Constant	1
Sum	$\xi^3+\xi'^3$
Hydrodynamic	$(\xi+\xi')^3$
Differential force	$(\xi+\xi')^2\lvert\xi^2-\xi'^2\rvert$

Two types of calculation were performed to investigate the predictive capabilities of LnEQMOM:

1. The moments of the rigorous NDF reported by Vanni (2000) were computed for each of the cases considered in this section. Numerical integration of the data extracted from the figures reported in Vanni (2000) was performed with the trapezoidal rule, in order to calculate these moments. The computed moments were then used as input to LnEQMOM to obtain the reconstructed NDF. Results were compared to the rigorous NDF and to the reconstruction obtained with Gamma EQMOM (Yuan et al., 2012).
2. The moment transport equations with LnEQMOM closures with the appropriate source terms were integrated to obtain the approximate distribution for each of the cases under consideration, starting from the initial conditions reported in the last column of Table 4.

Table 6
Breakup kernels.

Kernel	$a(\xi)$
Constant	1
Power law	ξ^{α}
Exponential	$e^{\delta\xi^3}$

Table 7
Daughter distribution functions and their moment transforms.

No.	Mechanism	$b(\xi\|\xi')$	$\overline{b}^k$
1	Symmetric fragmentation	$\begin{cases} 2, & \xi=\xi'/2^{1/3} \\ 0 & \text{otherwise} \end{cases}$	$2^{(3-k)/3}\xi^k$
2	Uniform	$\begin{cases} 6\xi^2/\xi'^3, & \xi\in]0,\xi'[\\ 0 & \text{otherwise} \end{cases}$	$6\xi^k/(k+3)$
3	Mass ratio 1 to 4	$\begin{cases} 1, & \xi=\xi'\left(\frac{1}{5}\right)^{1/3} \\ 1, & \xi=\xi'\left(\frac{4}{5}\right)^{1/3} \\ 0 & \text{otherwise} \end{cases}$	$\xi^k\frac{4^{k/3}+1}{5^{k/3}}$

This procedure was designed to isolate the error in the NDF reconstruction from the error due to the approximation in the time integration of the source terms that appear in the PBE. This is particularly relevant in some of the cases under examination, where the initial condition is characterized by a uniform NDF, which causes LnEQMOM to degenerate into QMOM, affecting the accuracy of the integration of the kernels.

Results obtained by integrating the moment equations with LnEQMOM were also compared to those previously obtained by Marchisio et al. (2003) using a three-node standard QMOM procedure. Time integration was performed with a two-stage Runge–Kutta method (RK-2), until a steady-state solution was achieved. For each case, the particle number density M_0, the mean particle size $d_{43}=M_4/M_3$, and the particle size distribution are reported.

Fig. 2 shows the results obtained for case 5 using LnEQMOM to reconstruct the NDF from the moments of the exact distribution reported in Vanni (2000), as a function of the number of nodes. LnEQMOM satisfactorily approximates the distribution function for large values of ξ when $N=1$ and $N=2$, however when a larger number of primary quadrature nodes are used, the reconstructed distribution shows oscillations that are not present in the rigorous

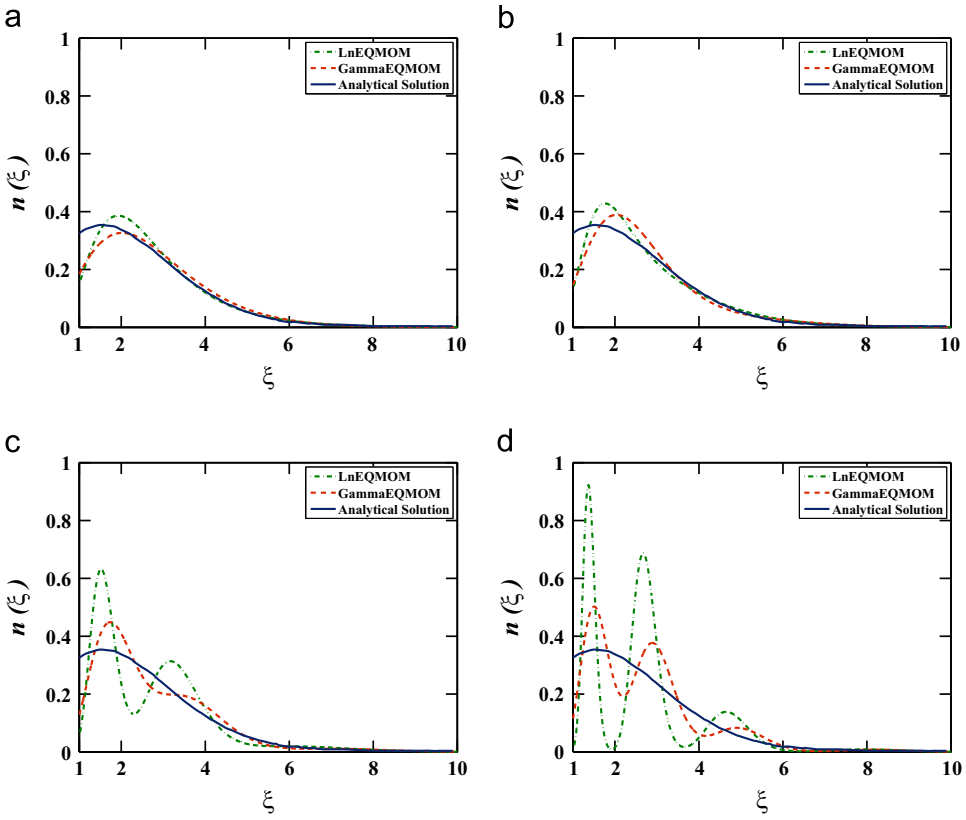

Fig. 2. Case 5 – Comparison of the reconstructed NDF from the exact moments of the rigorous solution of the PBE with LnEQMOM and Gamma EQMOM, as a function of the number of primary quadrature nodes N: (a) $N=1$; (b) $N=2$; (c) $N=3$; (d) $N=4$.

NDF. These oscillations originate from the summation of the kernel density functions. While they are undesirable because they compromise the shape of the reconstructed distribution, they do not directly affect the stability of the numerical simulation. In particular, the positivity of the NDF and its boundedness are guaranteed.

As expected, due to the functional form of the kernel function used in LnEQMOM, which rapidly tends to zero in the limit of $\xi \to 0^+$, the reconstructed NDF does not tend to the proper non-zero value of the rigorous solution at $\xi = 0$. This represents a limitation of the LnEQMOM procedure (and of any EQMOM procedure which relies on kernel density functions with the same

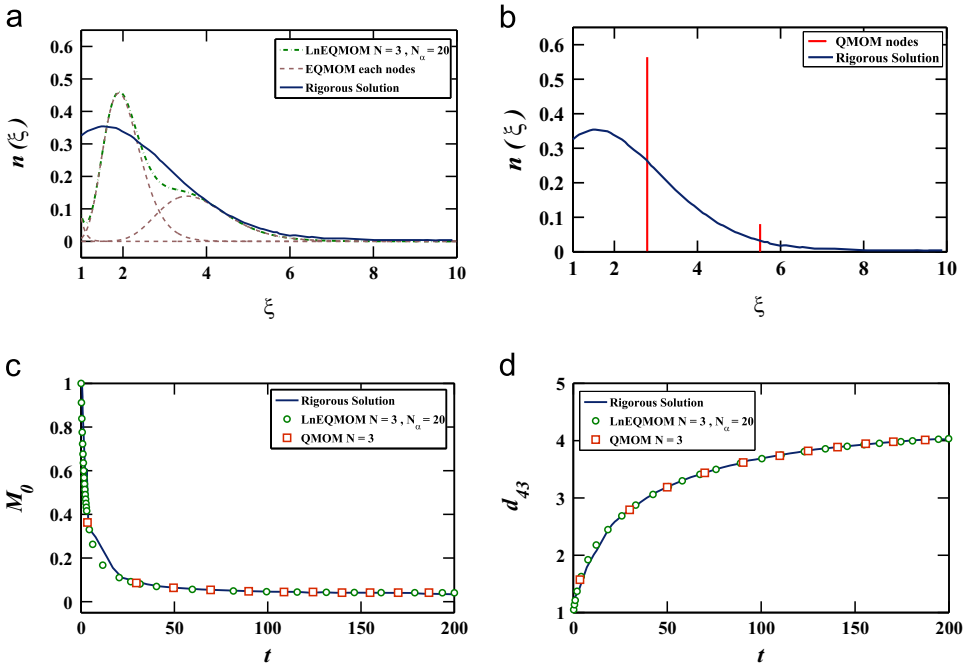

Fig. 3. Case 5 – (a) NDF from the rigorous solution and LnEQMOM, (b) NDF from the rigorous solution and QMOM, (c) zero-order moment of the NDF, (d) mean particle size d_{43}.

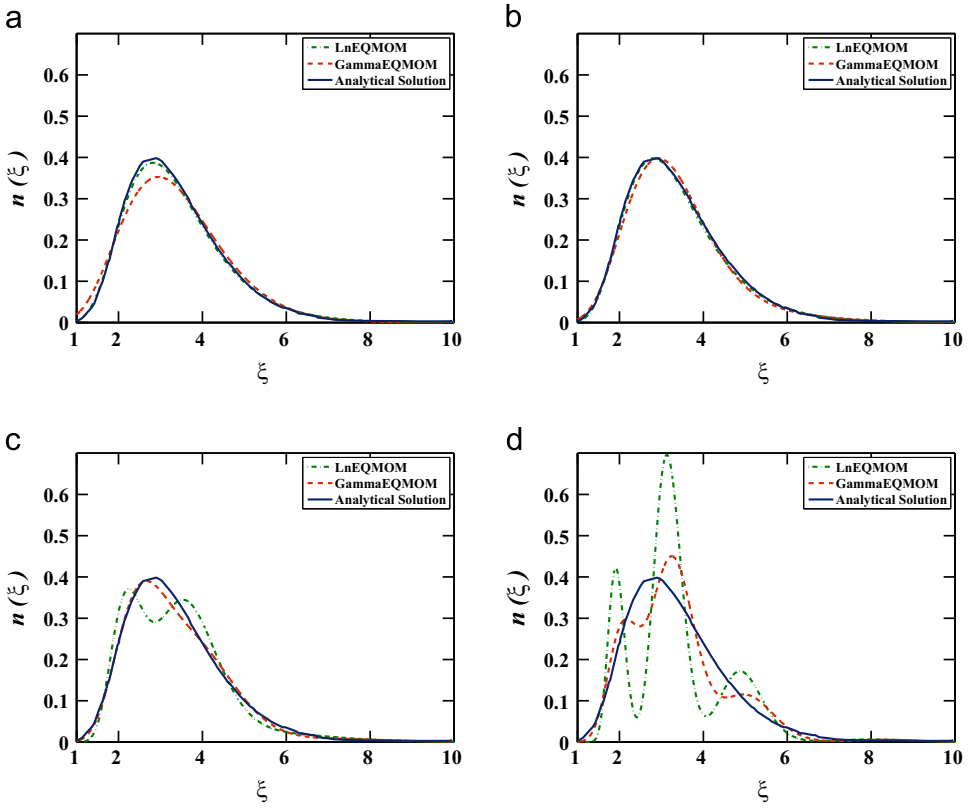

Fig. 4. Case 6 – Comparison of the reconstructed NDF from the exact moments of the rigorous solution of the PBE with LnEQMOM and Gamma EQMOM, as a function of the number of primary quadrature nodes N: (a) $N=1$; (b) $N=2$; (c) $N=3$; (d) $N=4$.

behavior for $\xi \to 0^+$), which is unable to accurately reconstruct distributions with finite non-zero value at $\xi = 0$, such as those appearing in cases involving evaporation. In such cases, the choice of the beta distribution is more appropriate, as shown in Yuan et al. (2012). However, even in this case, the reconstructed NDF has the same moments of the rigorous solution up to order $2N+1$, if a value for σ is found, Finally, we observe that similar predictions were obtained with Gamma kernel density functions.

Results obtained from the solution of the PBE with LnEQMOM for case 5 are reported in Fig. 3, for $t = 200$ s. As observed above, the right tail of the distribution is well captured by the approximate solution. However, important differences are observed for smaller values of ξ. Both QMOM and LnEQMOM (Fig. 3(c) and (d)) predict the time evolution of the particle number density M_0 and of the mean particle size d_{43} with comparable accuracy.

Results obtained with LnEQMOM and Gamma EQMOM applied to the moments of the rigorous solution for case 6 are reported in Fig. 4. In this case, two primary quadrature nodes are sufficient to obtain an excellent match of the reconstruction with the exact distribution, with the LnEQMOM results exactly overlapping the curve of the rigorous NDF. The reconstructed NDF provided by EQMOM with gamma kernel densities for this case is also in good agreement with the rigorous solution, but it shows larger differences compared to the result obtained with LnEQMOM. Fig. 5 shows the results obtained integrating the moment equations for case 6 in Table 4, where the sum aggregation kernel was used. The daughter distribution for symmetric fragmentation was adopted. The reconstructed distribution agrees well with the rigorous solution, however, the height of its peak is slightly overestimated. The time evolution of the total number density M_0 (Fig. 5(c)) is in excellent agreement with the rigorous solution, and with the QMOM prediction. Similar conclusions can be drawn for the time evolution of the particle mean diameter d_{43}, reported in Fig. 5(d).

Results concerning case 7 are reported in Figs. 6 and 7. The agreement between the reconstructed distribution obtained from the moments of the rigorous solution of the PBE and the rigorous solution itself is satisfactory. The tails of the distribution are well reproduced, however the shape of the central part of the distribution, and the maximum value of the NDF are not properly captured by the EQMOM procedure. The reconstructed NDF obtained integrating the moment transport equations (Fig. 7(a)) shows poorer agreement with the rigorous solution, if compared to the NDF reconstructed directly from the moments of the exact NDF. This may be caused by the accumulation of error during the integration process, in particular at the initial stages of the simulation, when the uniform initial condition forces the procedure to rely on the delta function representation of the NDF to integrate the source terms of the PBE. It is worth reminding that the EQMOM procedure smoothly and automatically degenerates into QMOM when a continuous reconstruction cannot be determined (Chalons et al., 2010; Yuan et al., 2012), allowing the calculation to proceed. The time evolution of the zero-order moment of the NDF (Fig. 7(c)), and of the mean diameter d_{43} (Fig. 7(d)) are in excellent agreement with those reported for the rigorous solution by Marchisio et al. (2003). Similar observations to those made for the reconstructed NDF of case 7 apply to case 8, as illustrated in Figs. 8 and 9. It is worth to highlight, however, that in this case the time evolution of the zero-order moment of the NDF (Fig. 9(c)) and of d_{43} (Fig. 9(d)) obtained with LnEQMOM show a significant improvement in comparison to the same quantities predicted by the standard QMOM procedure. In particular, the results provided by LnEQMOM for these two averaged quantities are in excellent agreement with those obtained with the rigorous solution of the PBE (Vanni, 2000), while those provided by QMOM (Marchisio et al., 2003) show a slight under-estimation of the zero-order moment and an important over-estimation of d_{43} for $t \in [0, 4]$. The reader should also notice that the predictions reported for cases 6–8 were obtained using two quadrature nodes for the EQMOM procedure, as opposed to the three quadrature nodes used in QMOM. As aconsequence, EQMOM not only provides a satisfactory reconstruction of the continuous NDF, and a significant improvement in the prediction of the time evolution of M_0 and d_{43} for cases 7 and 8, but it also allows a reduction of the number of quadrature nodes to be achieved. This positively

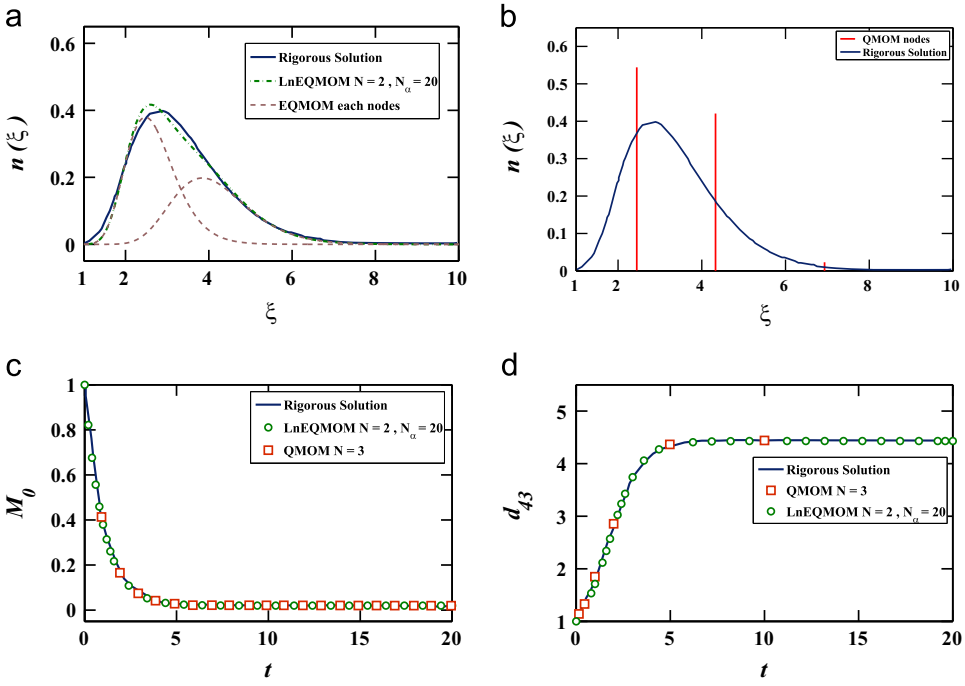

Fig. 5. Case 6 – (a) NDF from the rigorous solution and LnEQMOM, (b) NDF from the rigorous solution and QMOM, (c) zero-order moment of the NDF, (d) mean particle size d_{43}.

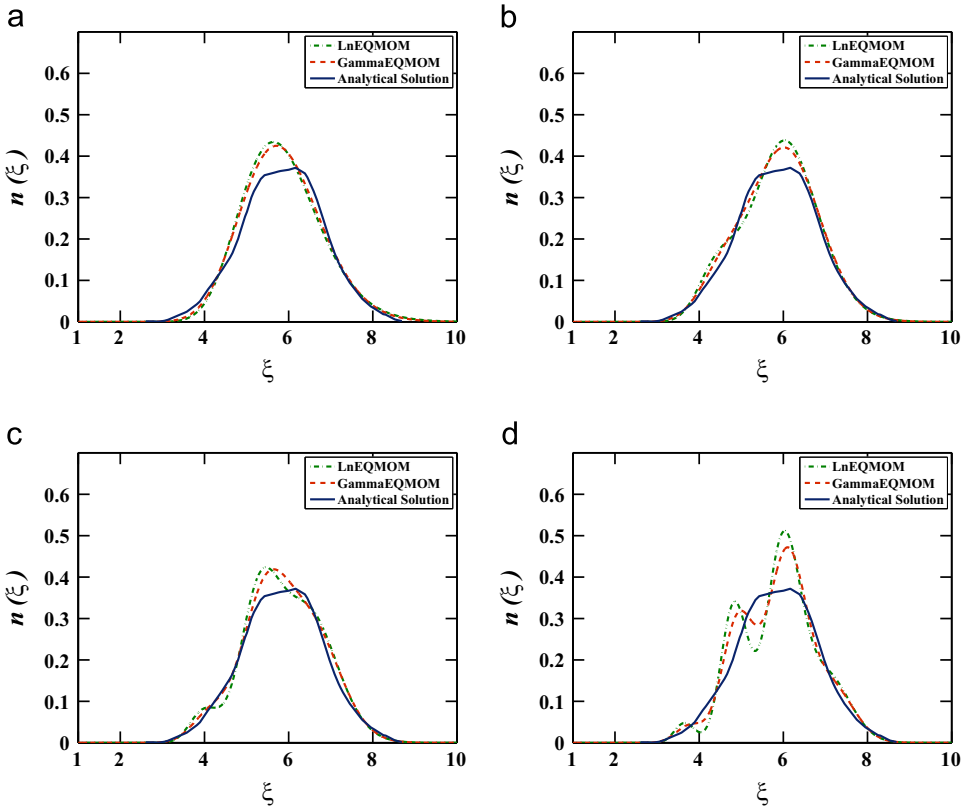

Fig. 6. Case 7 – Comparison of the reconstructed NDF from the exact moments of the rigorous solution of the PBE with LnEQMOM and Gamma EQMOM, as a function of the number of primary quadrature nodes N: (a) $N=1$; (b) $N=2$; (c) $N=3$; (d) $N=4$.

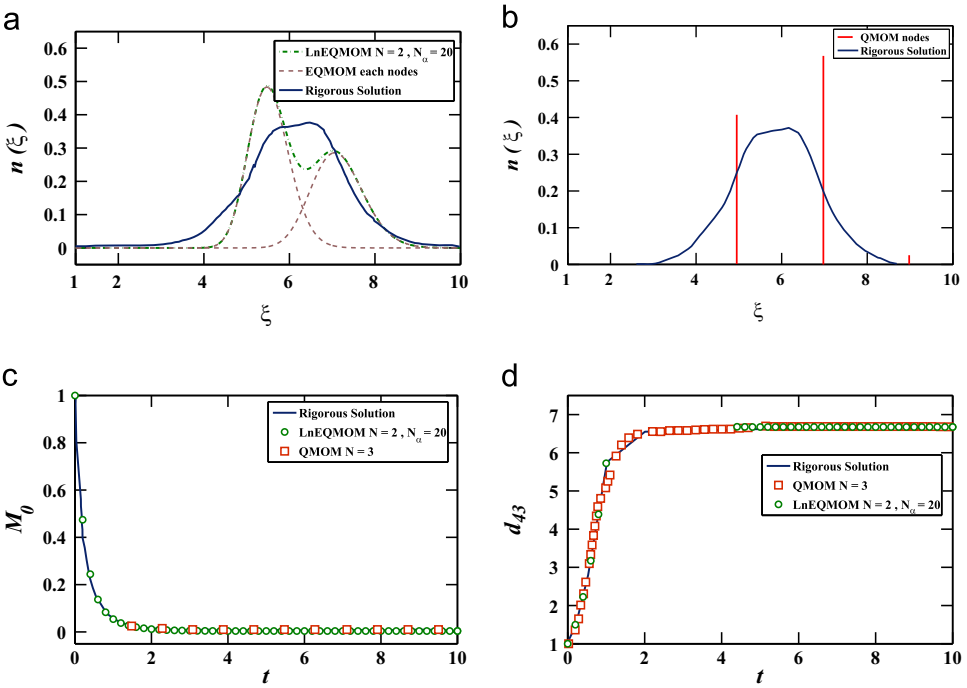

Fig. 7. Case 7 – (a) NDF from the rigorous solution and LnEQMOM, (b) NDF from the rigorous solution and QMOM, (c) zero-order moment of the NDF, (d) mean particle size d_{43}.

impacts the computational cost of the procedure, because the eigenproblem solved to perform the moment inversion involves a smaller matrix, and can be treated analytically.

LnEQMOM with $N=3$ and $N=4$ provides a satisfactory reconstruction of the NDF of case 9 (Fig. 10), when the moments of the rigorous NDF are used to perform the reconstruction. The cases with $N=1$ and $N=2$ are unable to reproduce the complex shape of the distribution, which presents three local maxima. As shown in Fig. 11, the NDF obtained by integrating the moment equations presents significant differences with respect to the rigorous

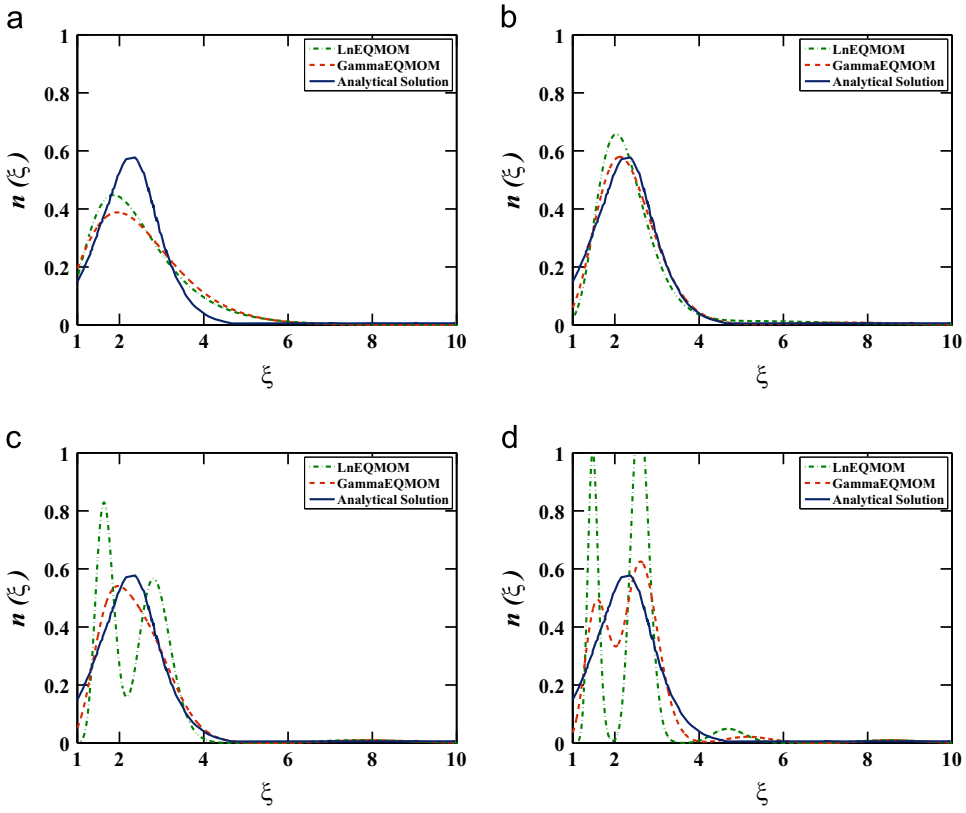

Fig. 8. Case 8 – Comparison of the reconstructed NDF from the exact moments of the rigorous solution of the PBE with LnEQMOM and Gamma EQMOM, as a function of the number of primary quadrature nodes N: (a) $N=1$; (b) $N=2$; (c) $N=3$; (d) $N=4$.

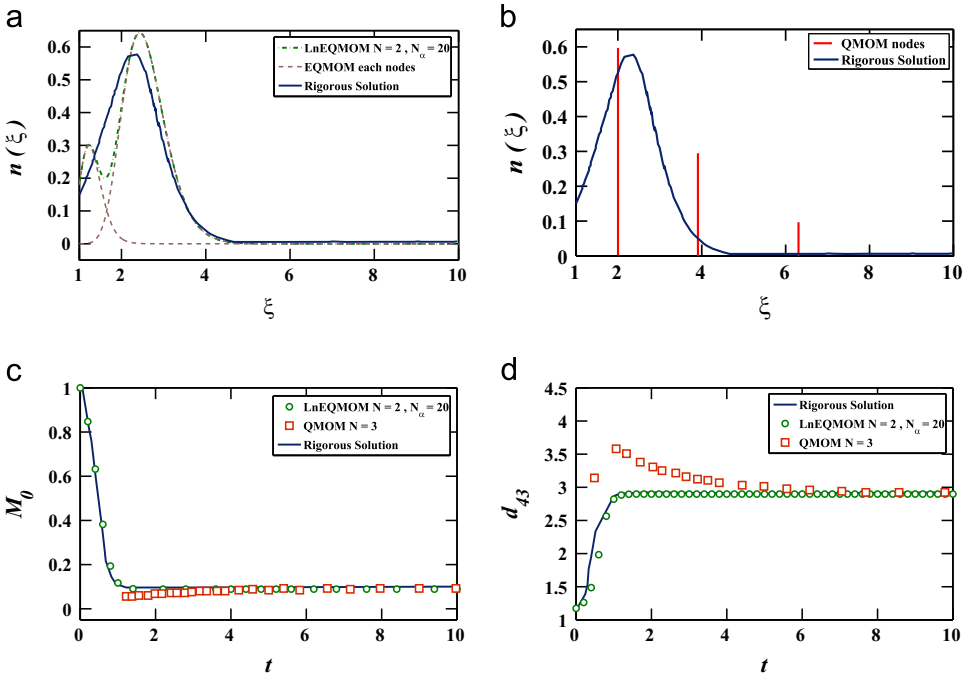

Fig. 9. Case 8 – (a) NDF from the rigorous solution and LnEQMOM, (b) NDF from the rigorous solution and QMOM, (c) zero-order moment of the NDF, (d) mean particle size d_{43}.

solution. However, the time evolution of the zero-order moment (Fig. 11(c)) and of the mean particle size d_{43} (Fig. 11(d)) are in excellent agreement with those obtained by Marchisio et al. (2003) for the rigorous solution.

4.3. Coalescence problem

We now consider a problem concerning coalescence, for which an analytical solution can be found. In this case $a(t,\xi,\xi')=\xi+\xi'$

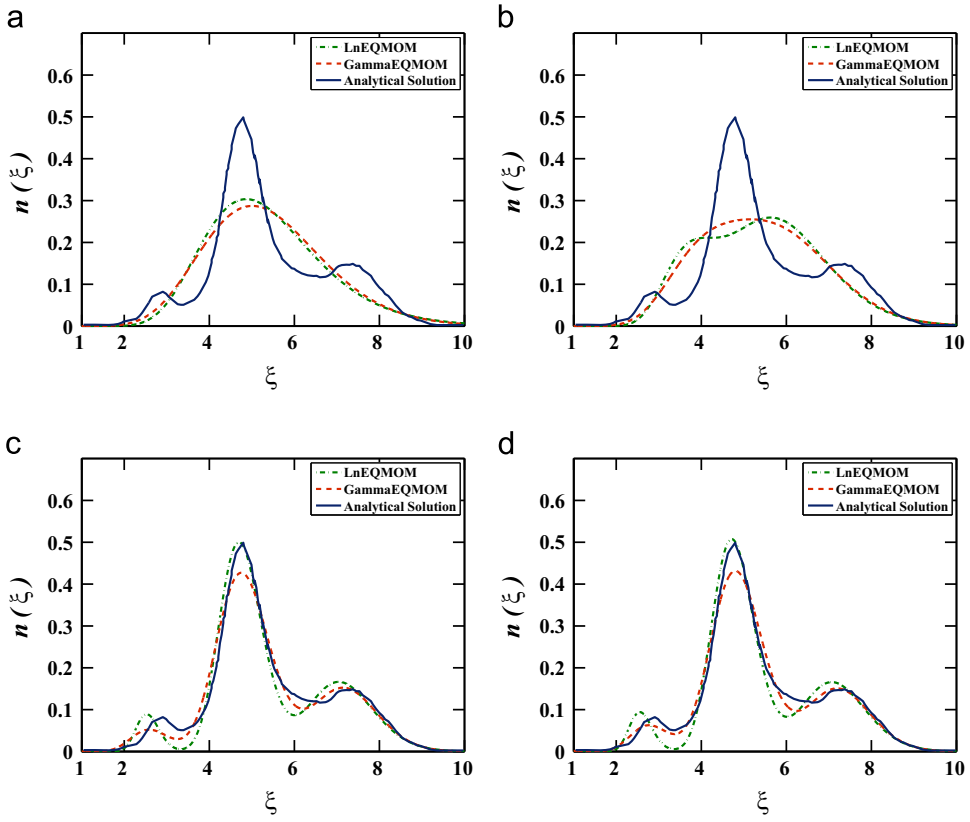

Fig. 10. Case 9 – Comparison of the reconstructed NDF from the exact moments of the rigorous solution of the PBE with LnEQMOM and Gamma EQMOM, as a function of the number of primary quadrature nodes N: (a) $N=1$; (b) $N=2$; (c) $N=3$; (d) $N=4$.

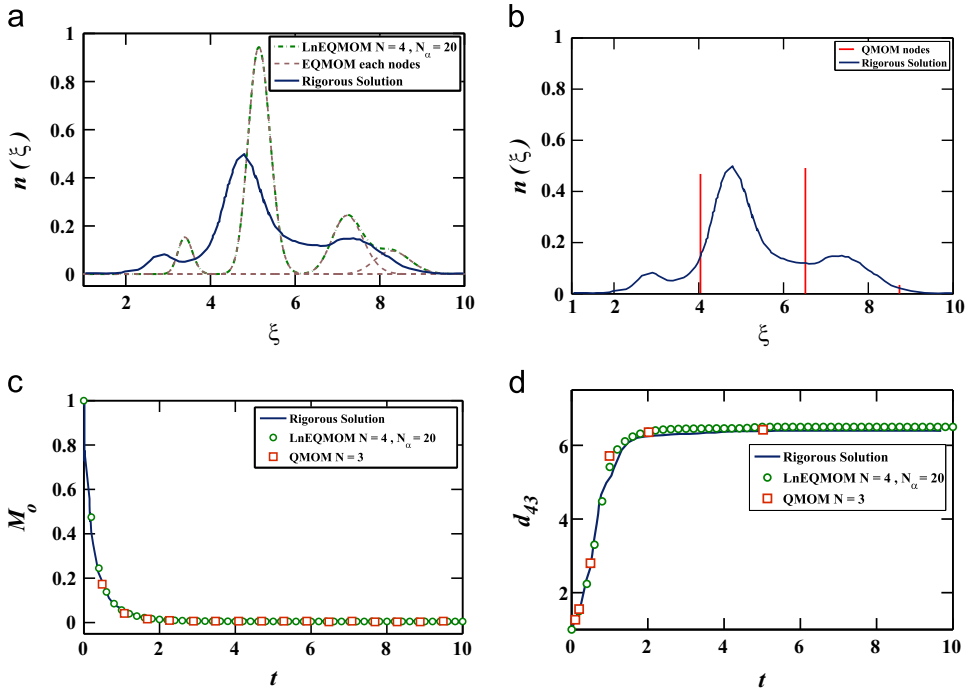

Fig. 11. Case 9 – (a) NDF from the rigorous solution and LnEQMOM, (b) NDF from the rigorous solution and QMOM, (c) zero-order moment of the NDF, (d) mean particle size d_{43}.

(sum kernel) is used, where ξ, the size variable, is volume. Since only coalescence is considered, no other kernel needs to be defined. The initial condition for this problem has been reported (Lage, 2011; Yuan et al., 2012) as

$$n(0,\xi) = \mathrm{e}^{-\xi}. \tag{29}$$

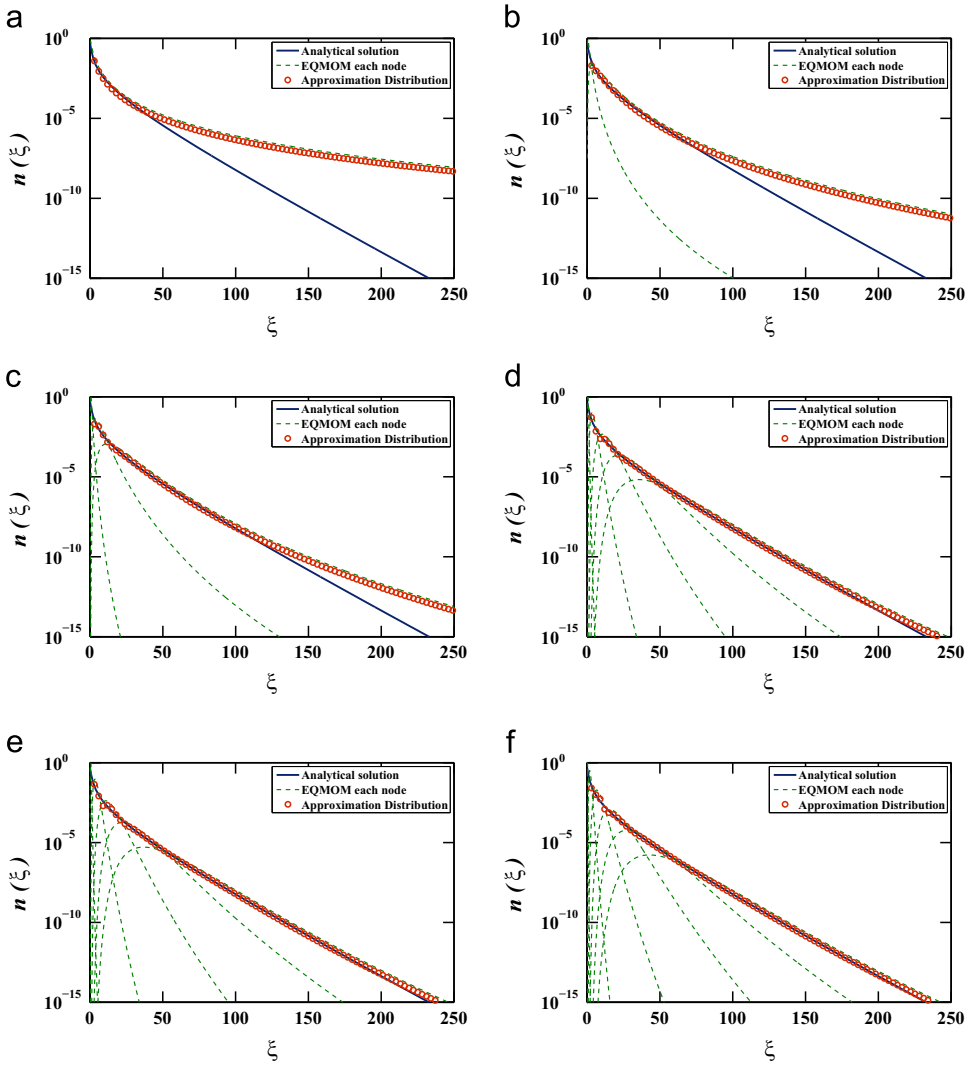

Fig. 12. Case 10 – Reconstructed distribution as a function of the number of nodes used in the primary quadrature obtained from the exact moments of the analytical solution: (a) $N=1$; (b) $N=2$; (c) $N=3$; (d) $N=5$; (e) $N=6$; (f) $N=7$.

The exact NDF for this problem is known (Gelbard and Seinfeld, 1978) and can be written as

$$n(t,\xi)=\frac{\mathrm{e}^{-t-2\xi+\xi\mathrm{e}^{-t}}}{\xi\sqrt{1-\mathrm{e}^{-t}}}I_1\left(2\xi\sqrt{1-\mathrm{e}^{-t}}\right), \tag{30}$$

where I_1 is the modified Bessel function. Results were obtained as a function of the number of primary quadrature nodes. The reconstructed NDF was obtained from the moments of the exact NDF, without integrating the moment transport equations. Increasing the number of primary quadrature nodes improves the accuracy of the reconstructed distribution, as illustrated in Fig. 12. The numerical approximation matches the analytical solution, properly predicting the slope of the tail of the distribution, and its behavior for large values of ξ.

4.4. Condensation problem

We consider here the reconstruction of the NDF in a condensation problem, where ξ is chosen to be particle volume. In this case, the PBE is (Yuan et al., 2012)

$$\frac{\partial n(\xi,\mathbf{x},t)}{\partial t}+\frac{\partial}{\partial\xi}\left[g(\xi,\mathbf{x},t)n(\xi,\mathbf{x},t)\right]=0, \tag{31}$$

and the corresponding moment transport equations are

$$\frac{\partial M_k(\mathbf{x},t)}{\partial t}=-g(\xi,\mathbf{x},t)n(\xi,\mathbf{x},t))\xi^k\Big|_0^{+\infty}+\int_0^{+\infty}k\xi^{k-1}g(\xi,\mathbf{x},t)n(\xi,\mathbf{x},t)\,\mathrm{d}\xi. \tag{32}$$

We consider the case in which $g(t,\xi)=\xi/2$, and with initial condition expressed as (Lage, 2011)

$$n(0,\xi)=6\xi^3\mathrm{e}^{-\xi}. \tag{33}$$

The exact NDF for this problem can be written as (Lage, 2011)

$$n(t,\xi)=\frac{\left(\xi\mathrm{e}^{-t/2}\right)^3\mathrm{e}^{-\xi\mathrm{e}^{-t/2}}}{6\mathrm{e}^{t/2}}. \tag{34}$$

The LnEQMOM reconstruction is only tested considering the exact moments of the analytical solution for brevity. Fig. 13 shows the LnEQMOM reconstruction obtained with an increased number of primary quadrature nodes. It is clear that increasing the number of the nodes will lead to more precise results for large values of ξ. However, oscillations appear when a large number of nodes are used. The reconstructed distribution agrees satisfactorily with the analytical solution, and the slope of its tail is properly captured by the reconstructed NDF.

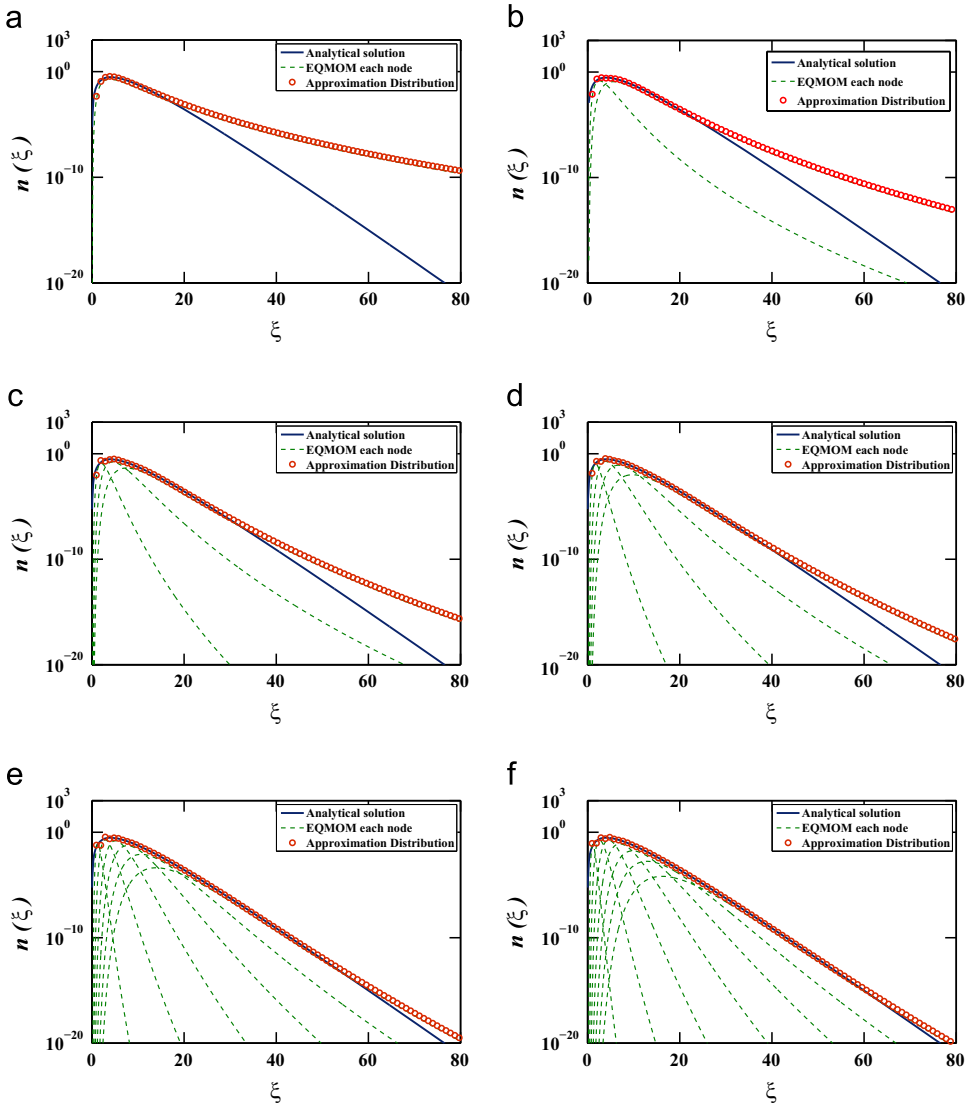

Fig. 13. Case 11 – Reconstructed distribution as a function of the number of nodes used in the primary quadrature obtained from the exact moments of the analytical solution: (a) $N=1$; (b) $N=2$; (c) $N=3$; (d) $N=5$; (e) $N=6$; (f) $N=7$.

Overall, the LnEQMOM procedure proved capable of accurately describing the moment evolution of the NDF in the cases we considered. However the reader should remember that, while the reconstructed distribution provided by LnEQMOM guarantees that the transported moments are preserved, the shape of the distribution does not necessarily match with the exact NDF that is solution of the original PBE. In most practical applications this does not represent an important limitation, because the quantities of interest to engineers are function of the moments of the NDF, however it should be taken into consideration whenever the result of interest is the reconstructed NDF itself.

4.5. Realizability of transformed moments

The LnEQMOM algorithm will succeed if the transformed moments are realizable. To this purpose, it is necessary to have an algorithm to check the moment realizability (Dette and Studden, 1997; Shohat and Tamarkin, 1943; Vikas et al., 2013; Yuan et al., 2012). A set of real values is a set of moments of a distribution function if the Hankel determinants are non-negative. The Hankel determinants for our case can be written as (Dette and Studden, 1997; Wright, 2007)

$$\Delta_{ij} = \begin{vmatrix} M^*_i & M^*_{i+1} & \cdots & M^*_{i+j} \\ M^*_{i+1} & M^*_{i+2} & \cdots & M^*_{i+j+1} \\ \vdots & \vdots & \ddots & \vdots \\ M^*_{i+j} & M^*_{i+j+1} & \cdots & M^*_{i+2j} \end{vmatrix}, \tag{35}$$

where $i=0,1$, $j=0,\ldots,N-1$. Fig. 14 shows the graphs for the target function $J(\sigma)$ and the graphs of the Hankel determinants as a function of σ for the case with $N=2$ primary quadrature nodes. In this case, the parameter σ is found solving Eq. (23). However, finding a root of Eq. (23) does not guarantee the realizability of the moment set $(M^*_0,\ldots,M^*_3)$. To this purpose, we examine the sign of the Hankel determinants to verify the set of moments M^*_i is realizable. The values of the parameter σ which set the target function J to zero are reported in the first column of Table 8. We indicate with σ_{H_0} and σ_{H_1} the values of σ which set the Hankel determinants $H_0=\Delta_{0,0}$ and $H_1=\Delta_{0,1}$ to zero. It is clear from the values reported in Table 8 that, for cases 5–9,

$$\sigma < \sigma_{H_0} \wedge \sigma < \sigma_{H_1}.$$

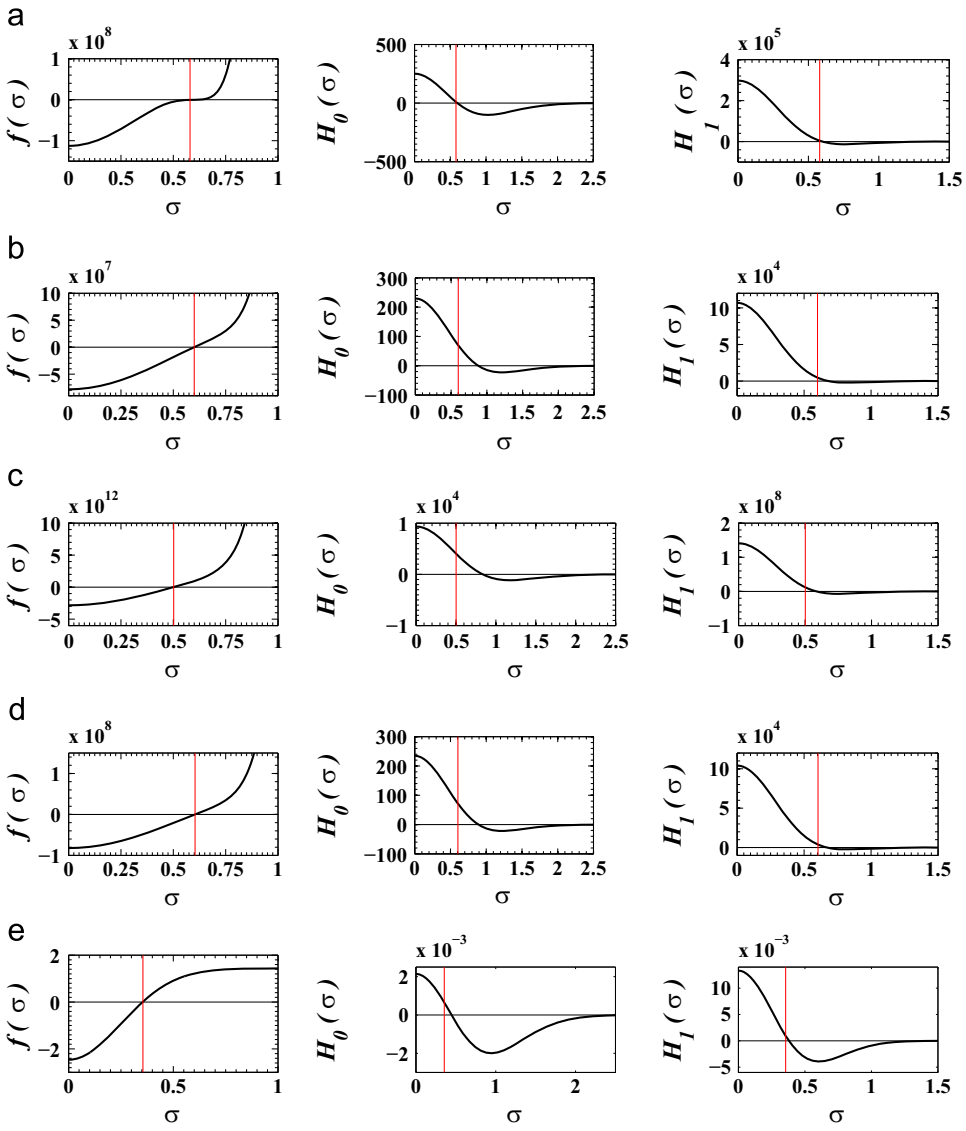

Fig. 14. Target function and Hankel determinants for cases 5–9 with $N=2$: (a) Case 5; (b) Case 6; (c) Case 7; (d) Case 8; (e) Case 9. (For interpretation of the references to color in the text, the reader is referred to the web version of this paper.)

Table 8
Values of σ, σ_{H_0}, and σ_{H_1} for cases 5–9.

Case	σ	σ_{H_0}	σ_{H_1}
5	0.580	0.624	0.612
6	0.600	0.881	0.682
7	0.502	0.836	0.586
8	0.604	0.893	0.672
9	0.355	0.450	0.381

Table 9
Normalized computational costs of the inversion algorithms.

Nodes	QMOM	LnEQMOM	gammaEQMOM
1	1	1.248	1.387
2	1	1.310	1.751
3	1	1.415	1.860
4	1	1.489	2.038

Examining Fig. 14, it is evident that both Hankel determinants H_0 and H_1 are positive for the value of σ at which $J=0$, indicated by the red vertical lines. As a consequence, the set of moments considered in the reconstruction is realizable for such a value of the parameter σ. Whether these determinants become negative, the moments will be non-realizable and the moment inversion procedure will fail. We generally choose the smallest positive value of σ which sets our target function to zero, as described in Yuan et al. (2012), however when such value leads to non-realizable moments, we search larger values of σ and choose one that ensures the realizability of the moment set.

5. Analysis of the computational costs

We show in this section an analysis of the computational costs associated to the EQMOM inversion procedure. The computational times required by one moment inversion using the log-normal and the gamma kernel density function are compared to the cost of the traditional QMOM procedure with Dirac delta functions. The computational time of QMOM is assumed to be 1, while the time required to complete one EQMOM moment inversion, including the root finding to determine the σ parameter, is normalized with

respect to the QMOM computational time. Table 9 reports the normalized computational times as a function of the number of quadrature nodes. These times were computed measuring the time required to perform a complete moment inversion in each of the cases considered in this work, and taking an average. It is worth to notice that the computational costs of the entire simulation may differ significantly from the costs of the moment inversion, depending on the closure used for the source terms in the PBE.

6. Conclusion

An extended quadrature method of moments with log-normal kernel density function (LnEQMOM) was presented in this study. The analytical solution to the cases with one and two primary nodes was studied, and a numerical procedure was described for cases involving larger number of quadrature nodes. The existence of at least one positive real value of the parameter σ was proven for the case with two primary quadrature nodes.

The proposed numerical approach was tested against cases concerning aggregation and breakup, coalescence, and condensation problems, demonstrating that LnEQMOM is capable of accurately predicting the time evolution of the zero-order moment and of the mean particle size in all the cases considered in this work, with results in excellent agreement with those obtained with the rigorous solution of the PBE, using a relatively low number of primary quadrature nodes ($N=2$ or 3 depending on the case). In particular, LnEQMOM provides more accurate results for the time evolution of the zero-order moment and of the mean particle size than QMOM for aggregation and breakup problems with symmetric and uniform daughter distributions (cases 7 and 8). This improvement is achieved using a lower number of primary quadrature nodes than the standard QMOM procedure.

Overall, satisfactory accuracy was achieved for what concerns the reconstructed number density function. In particular, LnEQMOM correctly predicts the tails of the NDF in the cases we considered. However, due to the functional form of the log-normal kernel, the method shows some difficulties in reconstructing distributions whose value for $\xi \to 0$ is not zero. LnEQMOM also appeared to be numerically more robust when compared to Gamma EQMOM, due to the structure of the system of equations used in the numerical procedure.

Some discrepancy was observed between the reconstructed NDF from the moments of the rigorous solution of the PBE, and the NDF obtained integrating in time the moment transport equations with LnEQMOM. This discrepancy may be attributed to the propagation of errors in the time-integration procedure, and to the fact that the uniform initial condition required delta functions to be used in the evaluation of the integrals involved in the source terms of the PBE. This aspect of the numerical procedure deserves a more in-depth study, in order to improve its accuracy, and it will be the object of future work.

Acknowledgments

The authors would like to thank Prof. Rodney O. Fox and Dr. Xiaofei Hu for the precious feedback they provided about this paper.

Appendix A. Numerical approximation of integrals in the PBE

We briefly summarize here the procedures to approximate the integrals that appear in the source terms of the PBE.

A.1. Gauss–Hermite quadrature

The first approach to perform the numerical integration of the source terms using known Gaussian quadrature formulae is to rely on a change of variable to reduce the quadrature problem to the well known case of Gaussian–Hermite quadrature (Gautschi, 2004). We illustrate the procedure considering the integral

$$\int_0^\infty g(\xi)\delta_\sigma(\xi,\mu)\,\mathrm{d}\xi = \int_0^\infty g(\xi)\frac{1}{\xi\sigma\sqrt{2\pi}}\mathrm{e}^{-(\ln\xi-\mu)^2/2\sigma^2}\,\mathrm{d}\xi. \tag{A.1}$$

We set

$$\frac{(\ln\xi-\mu)^2}{2\sigma^2} = s^2 \Rightarrow \xi = \mathrm{e}^{\sigma s\sqrt{2}+\mu}, \tag{A.2}$$

and so we can write the differential of ξ as

$$\mathrm{d}\xi = \sqrt{2}\sigma\mathrm{e}^{\sigma s\sqrt{2}+\mu}\,\mathrm{d}s. \tag{A.3}$$

Thus, the original integral becomes

$$\int_{-\infty}^\infty \frac{g\left(\mathrm{e}^{\sqrt{2}\sigma s+\mu}\right)\mathrm{e}^{-s^2}\sqrt{2}\sigma\mathrm{e}^{\sqrt{2}\sigma s+\mu}}{\mathrm{e}^{\sqrt{2}\sigma s+\mu}\sigma\sqrt{2\pi}}\,\mathrm{d}s = \frac{1}{\sqrt{\pi}}\int_{-\infty}^\infty g\left(\mathrm{e}^{\sqrt{2}\sigma s+\mu}\right)\mathrm{e}^{-s^2}\,\mathrm{d}s, \tag{A.4}$$

which can be approximated using standard Gauss–Hermite formula (Gautschi, 2004).

A.2. Gauss–Stieltjes–Wigert quadrature

The quadrature formula obtained in Appendix A.1 is exact for polynomials of $\psi = \ln x$. A quadrature formula exact for polynomials of x is obtained considering the Stieltjes–Wigert polynomials (Weisstein, 1998; Wilck, 2001), which are orthogonal to the log-normal distribution. The three-term recurrence relation that defines these polynomials is (Wilck, 2001)

$$P_{-1}=0, \quad P_0=1, \quad P_{i+1}=(x-a_i)P_i - b_iP_{i-1}, \quad i=1,2,\ldots, \tag{A.5}$$

where

$$\begin{aligned} &a_0=\eta, \quad a_i=\eta^{2i-1}\left[(\eta^2+1)\eta^{2i}-1\right],\\ &b_0=0, \quad b_i=\eta^{6i-4}(\eta^{2i}-1),\\ &\eta=\mathrm{e}^{\sigma^2/2}. \end{aligned} \tag{A.6}$$

The values of the quadrature weights and abscissae for both the approaches are found by solving an eigenvalue problem as explained in Wilf (1962), Golub and Welsch (1969), and Dette and Studden (1997).

We illustrate the procedure considering the integral

$$\int_0^\infty g(\xi)\delta_\sigma(\xi,\mu)\,\mathrm{d}\xi = \int_0^\infty g(\xi)\frac{1}{\xi\sigma\sqrt{2\pi}}\mathrm{e}^{-(\ln\xi-\mu)^2/2\sigma^2}\,\mathrm{d}\xi. \tag{A.7}$$

We set

$$\ln\xi-\mu = \ln s \Rightarrow \xi = s\mathrm{e}^{\mu},$$

and so we can write the differential of ξ as

$$\mathrm{d}\xi = \mathrm{e}^{\mu}\,\mathrm{d}s. \tag{A.8}$$

Thus the original integral becomes

$$\int_0^\infty \frac{g(s\mathrm{e}^{\mu})\mathrm{e}^{-\ln^2 s/2\sigma^2}\mathrm{e}^{\mu}}{s\mathrm{e}^{\mu}\sigma\sqrt{2\pi}}\,\mathrm{d}s = \int_0^\infty g(s\mathrm{e}^{\mu})w(s)\,\mathrm{d}s, \tag{A.9}$$

with

$$w(s) = \frac{\mathrm{e}^{-\ln^2 s/2\sigma^2}}{s\sigma\sqrt{2\pi}}. \tag{A.10}$$

References

Alopaeus, V., Laakskonen, M., Aittamaa, J., 2006. Solution of population balances with breakage and agglomeration by high-order moment-conserving method of classes. Chem. Eng. Sci. 61 (20), 6732–6752.

Alopaeus, V., Laakkonen, M., Aittamaa, J., 2008. Solution of population balances by high order moment-conserving method of classes: reconstruction of a non-negative density distribution. Chem. Eng. Sci. 63 (10), 2741–2751.

Athanassoulis, G.A., Gavriliadis, P.N., 2002. The truncated Hausdorff moment problem solved by using kernel density functions. Probab. Eng. Mech. 17 (3), 273–291.

Balakin, B.V., Hoffmann, A.C., Kosinski, P., 2014. Coupling STAR-CD with a population-balance technique based on the classes method. Powder Technol. 257, 47–54.

Bannari, R., Kerdouss, F., Selma, B., Bannari, A., Proulx, P., 2008. Three-dimensional mathematical modeling of dispersed two-phase flow using class method of population balance in bubble columns. Comput. Chem. Eng. 32 (12), 3224–3237.

Becker, P.J., Puel, F., Henry, R., Sheibat-Othman, N., 2011. Investigation of discrete population balance models and breakage kernels for dilute emulsification systems. Ind. Eng. Chem. Res. 50 (19), 11358–11374.

Bove, S., Solberg, T., Hjertager, B.H., 2005. A novel algorithm for solving population balance equations: the parallel parent and daughter classes. Derivation, analysis and testing. Chem. Eng. Sci. 60 (5), 1449–1464.

Capecelatro, J., Desjardins, O., Fox, R., 2014. Numerical study of collisional particle dynamics in cluster-induced turbulence. J. Fluid Mech. 747 R2-1–R2-13.

Chalons, C., Fox, R., Massot, M., 2010. A Multi-Gaussian Quadrature Method of Moments for Gas-particle Flows in a LES Framework. Studying Turbulence Using Numerical Simulation Databases, Center for Turbulence Research, Summer Program 2010, Stanford University, pp. 347–358.

Dette, H., Studden, W.J., 1997. The Theory of Canonical Moments with Applications in Statistics, Probability and Analysis. John Wiley & Sons.

Fox, R., Laurent, F., Massot, M., 2008. Numerical simulation of spray coalescence in an Eulerian framework: direct quadrature method of moments and multi-fluid method. J. Comput. Phys. 227 (6), 3058–3088.

Gautschi, W., 2004. Orthogonal Polynomials: Computation and Approximation. Oxford University Press.

Gelbard, F., Seinfeld, J.H., 1978. Numerical solution of the dynamic equation for particulate systems. J. Comput. Phys. 28 (3), 357–375.

Golub, G.H., Welsch, J.H., 1969. Calculation of Gauss quadrature rules. Math. Comput. 23 (106), 221–230.

Gordon, R.G., 1968. Error bounds in equilibrium statistical mechanics. J. Math. Phys. 9, 655–662.

Hounslow, M., Ryall, R., Marshall, V., 1988. Discretized population balance for nucleation, growth, and aggregation. AIChE J. 34 (11), 1821–1832.

Hounslow, M.J., 1990. A discretized population balance for continuous systems at steady state. AIChE J. 36 (1), 106–116.

Hulburt, H.M., Katz, S., 1964. Some problems in particle technology: a statistical mechanical formulation. Chem. Eng. Sci. 19 (8), 555–574.

Kah, D., Laurent, F., Massot, M., Jay, S., 2012. A high order moment method simulating evaporation and advection of a polydisperse liquid spray. J. Comput. Phys. 231 (2), 394–422.

Kumar, S., Ramkrishna, D., 1996a. On the solution of population balance equations by discretization—I. A fixed pivot technique. Chem. Eng. Sci. 51 (8), 1311–1332.

Kumar, S., Ramkrishna, D., 1996b. On the solution of population balance equations by discretization—II. A moving pivot technique. Chem. Eng. Sci. 51 (8), 1333–1342.

Lage, P.L.C., 2011. On the representation of QMOM as a weighted-residual method—the dual-quadrature method of generalized moments. Comput. Chem. Eng. 35 (11), 2186–2203.

Limpert, E., Stahel, W.A., Abbt, M., 2001. Log-normal distribution across the sciences: keys and clues. BioScience 51 (5), 341–352.

Lin, Y., Lee, K., Matsoukas, T., 2002. Solution of the population balance equation using constant-number Monte Carlo. Chem. Eng. Sci. 57 (12), 2241–2252.

Magnus, W., Oberhettinger, F., Soni, R.P., 1966. Formulas and Theorems for the Special Functions of Mathematical Physics. Springer-Verlag.

Marchisio, D.L., Fox, R.O., 2005. Solution of population balance using the direct quadrature method of moments. J. Aerosol Sci. 36 (1), 43–73.

Marchisio, D.L., Fox, R.O., 2013. Computational Models for Polydisperse Particulate and Multiphase Systems. Cambridge University Press.

Marchisio, D.L., Vigil, R., Fox, R.O., 2003. Quadrature method of moments for aggregation-breakage processes. J. Colloid Interface Sci. 258 (2), 322–334.

Massot, M., Laurent, F., Kah, D., de Chaisemartin, S., 2010. A robust moment method for evaluation of the disappearance rate of evaporating sprays. SIAM J. Appl. Math. 70 (8), 3203–3234.

McGraw, R., 1997. Description of aerosol dynamics by the quadrature method of moments. Aerosol Sci. Technol. 27 (2), 255–265.

Mead, L.R., Papanicolaou, N., 1984. Maximum entropy in the problem of moments. J. Math. Phys. 25 (8), 2404–2417.

Meimaroglou, D., Kiparissides, C., 2007. Monte Carlo simulation for the solution of the bi-variate dynamic population balance equation in batch particulate systems. Chem. Eng. Sci. 62 (1820), 5295–5299.

Muhr, H., David, R., Villermaux, J., Jezequel, P.H., 1996. Crystallization and precipitation engineering—VI. Solving population balance in the case of the precipitation of silver bromide crystals with high primary nucleation rates by using the first order upwind differentiation. Chem. Eng. Sci. 51 (2), 309–319.

Petitti, M., Nasuti, A., Marchisio, D.L., Vanni, M., Baldi, G., Mancini, N., Podenzani, F., 2010. Bubble size distribution modeling in stirred gas-liquid reactors with QMOM augmented by a new correction algorithm. AIChE J. 56 (1), 36–53.

Puel, F., Fvotte, G., Klein, J.P., 2003. Simulation and analysis of industrial crystallization processes through multidimensional population balance equations. Part 1: a resolution algorithm based on the method of classes. Chem. Eng. Sci. 58 (16), 3715–3727.

Ramkrishna, D., 2000. Population Balances: Theory and Applications to Particulate Systems in Engineering. Academic Press.

Randolph, A.D., Larson, M.A., 1988. Theory of Particulate Processes: Analysis and Techniques of Continuous Crystallization. Academic Press.

Rosner, D.E., Yu, S., 2001. MC simulation of aerosol aggregation and simultaneous spheroidization. AIChE J. 47 (3), 545–561.

Shohat, J.A., Tamarkin, J.D., 1943. The Problem of Moments. American Mathematical Soc.

Silva, L.F.L.R., Rodrigues, R.C., Mitre, J.F., Lage, P.L.C., 2010. Comparison of the accuracy and performance of quadrature-based methods for population balance problems with simultaneous breakage and aggregation. Comput. Chem. Eng. 34 (3), 286–297.

Smith, M., Matsoukas, T., 1998. Constant-number Monte Carlo simulation of population balances. Chem. Eng. Sci. 53 (9), 1777–1786.

Strumendo, M., Arastoopour, H., 2008. Solution of PBE by MOM in finite size domains. Chem. Eng. Sci. 63 (10), 2624–2640.

Tagliani, A., 1999. Hausdorff moment problem and maximum entropy: a unified approach. Appl. Math. Comput. 105 (23), 291–305.

Vanni, M., 2000. Approximate population balance equations for aggregation-breakage processes. J. Colloid Interface Sci. 221 (2), 143–160.

Vie, A., Laurent, F., Massot, M., 2013. Size-velocity correlations in hybrid high order moment/multi-fluid methods for polydisperse evaporating sprays: modeling and numerical issues. J. Comput. Phys. 237, 177–210.

Vikas, V., Hauck, C., Wang, Z., Fox, R., 2013. Radiation transport modeling using extended quadrature method of moments. J. Comput. Phys. 246, 221–241.

Weisstein, E.W., 1998. CRC Concise Encyclopedia of Mathematics. CRC Press.

Wheeler, J.C., 1974. Modified moments and Gaussian quadratures. Rocky Mt J. Math. 4, 287–296.

Wilck, M., 2001. A general approximation method for solving integrals containing a lognormal weighting function. J. Aerosol Sci. 32 (9), 1111–1116.

Wilf, H.S., 1962. Mathematics for the Physical Sciences. Wiley.

Wright, D.L., 2007. Numerical advection of moments of the particle size distribution in Eulerian models. J. Aerosol Sci. 38 (3), 352–369.

Yuan, C., Laurent, F., Fox, R., 2012. An extended quadrature method of moments for population balance equations. J. Aerosol Sci. 51, 1–23.

Zhao, H., Maisels, A., Matsoukas, T., Zheng, C., 2007. Analysis of four Monte Carlo methods for the solution of population balances in dispersed systems. Powder Technol. 173 (1), 38–50.

Zhao, H., Zheng, C., 2013. A population balance-Monte Carlo method for particle coagulation in spatially inhomogeneous systems. Comput. Fluids 71, 196–207.